Article

Autoregulation of the Rsc4 Tandem Bromodomain by Gcn5 Acetylation

Andrew P. VanDemark,[1,6] Margaret M. Kasten,[2,3,4,6] Elliott Ferris,[1] Annie Heroux,[5] Christopher P. Hill,[1,*] and Bradley R. Cairns[2,3,4,*]
[1]Department of Biochemistry, University of Utah School of Medicine, Salt Lake City, UT 84112, USA
[2]Howard Hughes Medical Institute
[3]Department of Oncological Sciences
[4]Huntsman Cancer Institute
University of Utah School of Medicine, Salt Lake City, UT 84112, USA
[5]Department of Biology, Brookhaven National Laboratory, Upton, NY 11973, USA
[6]These authors contributed equally to this work.
*Correspondence: brad.cairns@hci.utah.edu (B.R.C.), chris@biochem.utah.edu (C.P.H.)
DOI 10.1016/j.molcel.2007.08.018

SUMMARY

An important issue for chromatin remodeling complexes is how their bromodomains recognize particular acetylated lysine residues in histones. The Rsc4 subunit of the yeast remodeler RSC contains an essential tandem bromodomain (TBD) that binds acetylated K14 of histone H3 (H3K14ac). We report a series of crystal structures that reveal a compact TBD that binds H3K14ac in the second bromodomain and, remarkably, binds acetylated K25 of Rsc4 itself in the first bromodomain. Endogenous Rsc4 is acetylated only at K25, and Gcn5 is identified as necessary and sufficient for Rsc4 K25 acetylation in vivo and in vitro. Rsc4 K25 acetylation inhibits binding to H3K14ac, and mutation of Rsc4 K25 results in altered growth rates. These data suggest an autoregulatory mechanism in which Gcn5 performs both the activating (H3K14ac) and inhibitory (Rsc4 K25ac) modifications, perhaps to provide temporal regulation. Additional regulatory mechanisms are indicated as H3S10 phosphorylation inhibits Rsc4 binding to H3K14ac peptides.

INTRODUCTION

Chromatin serves a central role in regulating the access of transcription factors to chromosomal loci. The primary repeating unit of chromatin, the nucleosome, helps organize DNA topology by wrapping DNA, a property that can occlude binding sites for regulatory factors and thereby contribute to transcriptional silencing (Kornberg and Lorch, 1999). However, the nucleosome is a dynamic participant in transcriptional activation, because nucleosome remodelers function to reposition nucleosomes to expose the underlying DNA. Furthermore, a large array of covalent modifications occur on the histone components and can serve as binding epitopes for protein domains specialized for their recognition. The principle of histone marking by covalent modification and recognition by specific domains has been termed "the histone code" (Fischle et al., 2003; Strahl and Allis, 2000). These binding domains reside on both chromatin regulators and transcriptional regulators. Thus, most factors are targeted to particular locations in the genome by one of two mechanisms: through interactions with site-specific DNA binding proteins or by using specialized domains to interact with modified histones. The most common posttranslational modification of histones is the acetylation of lysine residues by histone acetyltransferase (HAT) enzymes, which occurs primarily on the flexible N-terminal histone "tails" that emanate from the globular nucleosome core (Kouzarides, 2000). One of the best-studied HAT enzymes is yeast Gcn5, which acetylates lysine 14 of histone H3 (H3K14ac), a modification correlated with transcriptional activation (Brownell et al., 1996; Howe et al., 2001; Lo et al., 2000; Syntichaki et al., 2000; Trievel et al., 1999). Acetylated lysines are typically bound by ~110 amino acid residue structures called bromodomains that also recognize several of the residues flanking the acetyl-lysine, thereby providing acetyl-lysine recognition within a sequence context (Hudson et al., 2000; Mujtaba et al., 2002; Owen et al., 2000). There is considerable interest in determining which bromodomains bind particular histone acetyl-lysines and whether these interactions mediate targeting or some other aspect of regulation.

Complexes that rely on bromodomains for their full function include chromatin remodelers, which use the energy of ATP hydrolysis to move and/or eject nucleosomes to uncover the underlying DNA (Cairns, 2005). Indeed, how remodelers are targeted and regulated is a central question in chromatin biology. Important initial work demonstrated that bromodomains present on the yeast remodeler SWI/SNF are important for the retention of the remodeler on acetylated chromatin templates, consistent with a role for bromodomains in targeting (Hassan et al., 2002, 2006). The paralog of ySWI/SNF is the 15 subunit remodels

the structure of chromatin (RSC) complex, which is both abundant and essential in *S. cerevisiae* (Cairns et al., 1996) and is involved in multiple chromosomal processes including transcriptional regulation, DNA repair, stress response, and chromosome cohesion and segregation (Angus-Hill et al., 2001; Baetz et al., 2004; Cairns et al., 1999; Chai et al., 2005; Chang et al., 2005; Yukawa et al., 1999). Importantly, RSC subunits contain 8 of the 15 bromodomains in *S. cerevisiae*, indicating that histone acetylation likely plays a central role in recruiting RSC to chromatin and/or in regulating its remodeling activity. Consistent with this notion, acetylation of histones promotes nucleosome remodeling by RSC and the passage of RNA polymerase II through chromatin in vitro (Carey et al., 2006).

The Rsc4 subunit of the RSC complex, which contributes to RSC-activated Pol II transcription in vivo (Kasten et al., 2004; Soutourina et al., 2006), contains a pair of bromodomains, termed BD1 and BD2, that are essential for cell viability (Kasten et al., 2004). BD1 and BD2 are adjacent in the primary protein sequence and together form the Rsc4 tandem bromodomain (TBD, residues 56–304). Our previous studies indicated that the Rsc4 TBD binds H3K14ac (Kasten et al., 2004). For example, the Rsc4 TBD preferentially binds histone H3 N-terminal peptides acetylated at K14, but not at several other positions tested on both the H3 and the H4 tails. Furthermore, conditional *rsc4* alleles are lethal in combination with *gcn5Δ* (Gcn5 acetylates H3K14) or with *h3k14* replacements (at 33°C), but not in combination with mutation of other lysine residues in the H3 and H4 tails (Kasten et al., 2004). However, it was unresolved which of the bromodomains (or both) bound H3K14ac, and the clear possibility remained of alternative ligands. Furthermore, it was not known whether other modifications occurring near H3K14ac, such as H3S10 phosphorylation, might affect binding.

To better understand Rsc4 recognition of chromatin, we performed biochemical and genetic studies that showed that only BD2 binds to H3K14ac peptides, and we visualized the acetyl lysine component of this interaction using X-ray crystallography. Serendipitously, crystal structure determination of protein prepared by in vitro acetylation with Gcn5 revealed that an acetylated lysine of Rsc4(K25ac) binds to its own BD1. This interaction was shown to be important in vivo, and the modifying enzyme was identified as Gcn5, the same acetyltransferase that modifies the H3K14 ligand of BD2. Importantly, peptide-binding data showed that binding of Rsc4 K25ac to BD1 impairs the ability of BD2 to bind an H3K14ac peptide, thereby indicating an autoregulation mechanism for recognition of a histone modification.

RESULTS AND DISCUSSION

### Structure of the Rsc4 Tandem Bromodomain

Several crystal structures of Rsc4 constructs were determined (Figure 1). The first, Rsc4(36–340), was determined by the SAD method using selenomethionine-substituted protein and refined to a free R value of 21.8% against na-

tive data to 1.8 Å resolution. This structure is ordered from residue 36 to residue 320 with no disordered internal loops. Structures of other constructs were subsequently determined by molecular replacement and refined to resolutions of 1.75–2.35 Å and R_{free} values of 21.9%–24.8%. While the structures varied significantly in their last ordered residue (313–320), only minor differences were seen for residues 36–312, with root-mean-square deviations (rmsds) of 0.5–1.0 Å following least-squares overlap on 275 pairs of Cα atoms.

The Rsc4 TBD is a compact structure in which each of the individual bromodomains (BD1 and BD2) resembles bromodomains from other proteins (Mujtaba et al., 2002; Owen et al., 2000; Sun et al., 2007). In keeping with standard nomenclature, we name the four bundle helices Z, A, B, and C, with a -1 or -2 suffix to indicate if it is from the first or second bromodomain (Figure 1C). The acetyl-lysine binding pockets are formed primarily by residues within the BC and ZA loops including the short helix Z'. Both BD1 and BD2 conserve two tyrosine residues within Z' and an asparagine residue within B that are characteristic of bromodomain binding sites. Overlap on Cα atoms with the bromodomain from Gcn5, which shares 19% and 33% sequence identity with Rsc4 BD1 and BD2, respectively, and whose crystal structure has been determined at 1.9 Å resolution (Owen et al., 2000), gives rmsds of 1.8 Å (100 pairs of Cα atoms) for BD1 and 1.6 Å (106 pairs of Cα atoms) for BD2.

The Rsc4 TBD reveals important differences with the previously reported structure of the double bromodomain of $TAF_{II}1$ (formerly termed $Taf_{II}250$) (Jacobson et al., 2000), the largest subunit of the TBP-associated factors for RNA Pol II transcription. We note that $TAF_{II}1$ was only crystallized in the absence of ligand. Notably, the relative positions and orientations of the two bromodomains in Rsc4 are very different to those in $TAF_{II}1$ (see Figure S1 in the Supplemental Data available with this article online). Also, Rsc4 is substantially more compact, with extensive BD1-BD2 interactions (mainly through αC-1 and αB-2) that bury a total of 1621 Å^2 of solvent accessible surface area at the bromodomain interface (Figure S2). In comparison, 1122 Å^2 are buried at the BD1-BD2 interface in the $TAF_{II}1$ structure. This supports the impression from genetic data that the Rsc4 TBD functions as a single structural unit (Kasten et al., 2004). In contrast, the two bromodomains of $TAF_{II}1$ appear to be relatively independent. As a result of these differences, the two acetyl-lysine binding sites of Rsc4 face the same side of the structure in the same relative orientation and are separated by just 20 Å.

Whereas BD1 conforms to the standard bromodomain architecture, BD2 includes an additional "wing" helix (W) inserted between Z-2 and A-2. Because it is adjacent to the presumed binding surface, we hypothesized that W might play an important functional role. We therefore designed a deletion variant that replaced residues 187–206 with a short Ser-Ser-Gly linker, termed *rsc4Δ187–206*. Although the *rsc4Δ187–206* allele does not confer a strong phenotype in isolation, a temperature-sensitive (ts⁻)
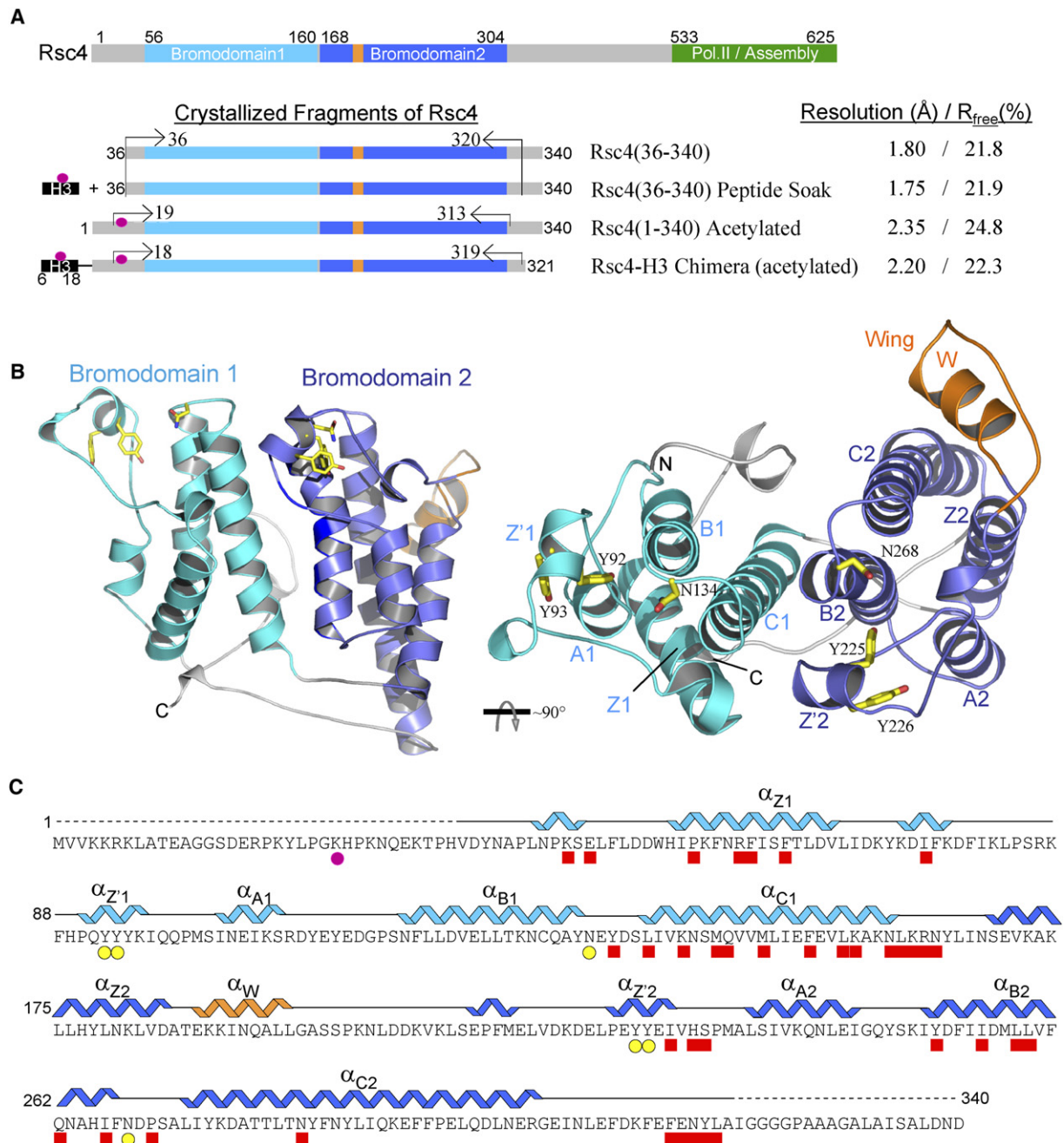
Figure 1. Structures of Rsc4

(A) Domain organization of Rsc4 (top) and crystallized constructs (bottom). Rsc4 structure is the following: bromodomain 1 (cyan), bromodomain 2 (blue), wing insertion (orange), and the binding region for RSC and the RNA polymerases (green) (Kasten et al., 2004; Soutourina et al., 2006). First and last ordered residues in the crystallized constructs are indicated with arrows. Acetylated lysine residues are indicated with a magenta dot (K14 of H3 and K25 of Rsc4).

(B) Orthogonal views of Rsc4(36–340) ribbon diagram. Secondary structures are labeled, and termini are indicated N and C. The asparagine and two tyrosine side chains from each bromodomain that are important for acetyl lysine binding are colored yellow. The wing insertion is colored orange.

(C) Rsc4 amino acid sequence with secondary structures indicated above. Residues not ordered in the Rsc4(36–340) structure are indicated with a dashed line. The red squares indicate interface residues between BD1 (residues 36–162) and BD2 (residues 163–320). The magenta circle indicates the site of acetylation (K25).

phenotype was conferred in combination with *gcn5Δ* (data not shown), suggesting that the wing might assist BD2 in H3K14ac recognition.

H3K14ac Binds Preferentially to Rsc4 BD2

We took both in vivo and in vitro approaches to determine which of the two Rsc4 bromodomains binds H3K14ac. Our in vivo approach involved isolating mutations specifically impaired at individual bromodomains and testing them in combination with *gcn5Δ* and *h3K14* mutations. First, we made mutations in BD1 or BD2 of two tyrosine residues that are highly conserved in all bromodomains (Figure S3) and are important for recognizing the acetyl moiety in acetyl-lysine. Replacement of these tyrosines with alanine resulted in the *rsc4* alleles *rsc4* Y92A Y93A (BD1 mutant), *rsc4* Y225A Y226A (BD2 mutant), and the combined *rsc4* Y92A Y93A Y225A Y226A (BD1&2 mutant) alleles. Each encoded a stable derivative that was fully capable of assembly into the RSC complex (data not shown). The isolated BD mutant alleles lack clear plate phenotypes, likely due to the fact that the normal interaction of bromodomains with their substrates involves an interaction with the acetyl moiety (which is compromised) and also the peptide sequence (which is retained). However, the combined BD1&2 mutations conferred lethality (even in WT *GCN5* background, Figure 2A). This demonstrates that the two bromodomains are partially redundant; compromising the acetyl-binding pocket of both bromodomains is needed to confer inviability. We note that redundancy can result from the two bromodomains binding to different ligands; compromising one bromodomain makes Rsc4 reliant on the alternative bromodomain and its ligand(s) to conduct an essential function.

In support of the two bromodomains binding different ligands, we found that *rsc4* Y92A Y93A *gcn5Δ* combinations were lethal, whereas *rsc4* Y225A Y226A *gcn5Δ* combinations grew well (Figure 2A). As above, lethality could result from compromising both BD1 and BD2; BD1 is compromised through mutation of the tyrosine residues and BD2 through the lack of the acetyl group on the H3K14 substrate in the *gcn5Δ* background. Consistent with this notion, synthetic lethality was also observed when the BD1 mutant was combined with the *h3*K14G mutant (Figure 2A). These data implicate BD2 in binding H3K14ac, because mutations in BD2 that prevent the recognition of the acetyl moiety (Y225A, Y226A) are not expected to be exacerbated by the absence of the acetyl group on the substrate (from *gcn5Δ*). In contrast, the synthetic lethality observed by combining a BD1 mutation with *gcn5Δ* implicates an important function for BD1 in binding a ligand(s) distinct from H3K14ac.

An NMR titration experiment indicated that the Rsc4-H3K14ac peptide dissociation constant is approximately 1–2 mM (data not shown). This low inherent binding is not unusual for bromodomains (Hudson et al., 2000; Shen et al., 2007; Sun et al., 2007) and presumably reflects the involvement of additional contacts with the nucleosome in the context of the intact RSC complex. It does,

however, limit the choice of binding assay, and we therefore estimated relative binding affinities using biotinylated H3 tail peptides (residues 1–39) that were either acetylated at K14 or unmodified, and were immobilized on streptavidin beads. This analysis revealed that Rsc4(46–334) binds H3K14ac peptides in preference to unmodified peptides (Figure 2B). Consistent with the genetic experiments, the Y92F variant (intact BD2) binds H3K14ac peptides preferentially in the same manner as the wild-type (WT) sequence, whereas preferential binding is abolished with the equivalent mutation in BD2 (Y225F) (Figure 2B). Moreover, a Rsc4(157–321) BD2 derivative that lacked BD1 entirely still demonstrated a preferential interaction with H3K14ac peptides compared to unmodified peptides (Figure 2C). Not surprisingly, given the extensive interactions between BD1 and BD2, peptide binding to the isolated BD2 structure was weaker than to the TBD, and the isolated BD1 was insoluble (data not shown). The binding assay was further used to map the Rsc4 interaction to residues 6–21 of the H3K14ac peptide, with further truncation from the N terminus preventing binding to the intact Rsc4(36–321) (data not shown). Thus, these data indicate that Rsc4 BD2 preferentially binds the H3 tail acetylated at K14 with other interactions also contributing to binding affinity. We also examined whether or not modifications near H3K14 affect H3K14ac recognition. Previous work suggested that H3K9 acetylation does not affect Rsc4 binding (Kasten et al., 2004). However, S10 phosphorylation has previously been linked to H3K14 acetylation (Lo et al., 2000) and had not been examined in our prior studies. We find that S10 phophorylation antagonizes selective binding of Rsc4(36–321) to H3K14ac peptides, raising the possibility that this modification may restrict RSC binding in vivo (Figure 2D).

Structure of Rsc4 BD2 Bound to H3K14ac

To visualize the H3-Rsc4 interaction, we determined the structure of a peptide complex by soaking Rsc4(36–340) crystals in high concentrations (~40 mM) of H3(6–18)K14ac (Table 1). Density for the peptide backbone is not apparent in this 1.7 Å resolution structure but is clearly defined for an acetylated lysine side chain in the BD2 binding site in a conformation that overlaps closely with the structure of a Gcn5 bromodomain ligand complex (Figure 2E). Unfortunately, density was not reliably interpretable beyond the side chain, and it was not possible to determine the path of the bound peptide backbone. Numerous data sets were obtained and structures determined at 1.7–2.3 Å resolution for Rsc4(36–340) cocrystallized or soaked with H3 peptide, but ligand density was always limited to the Kac side chain. The BD1 and BD2 pockets are open in the crystal lattice, although they are each within 6 Å of significant crystal contacts. Because in vitro binding appears normal in the 6–21 H3K14ac peptide but is abolished in a 10–21 peptide (data not shown), it seems likely that lattice contacts prevent secondary interactions that are important for full binding affinity and block the peptide from adopting the bound conformation
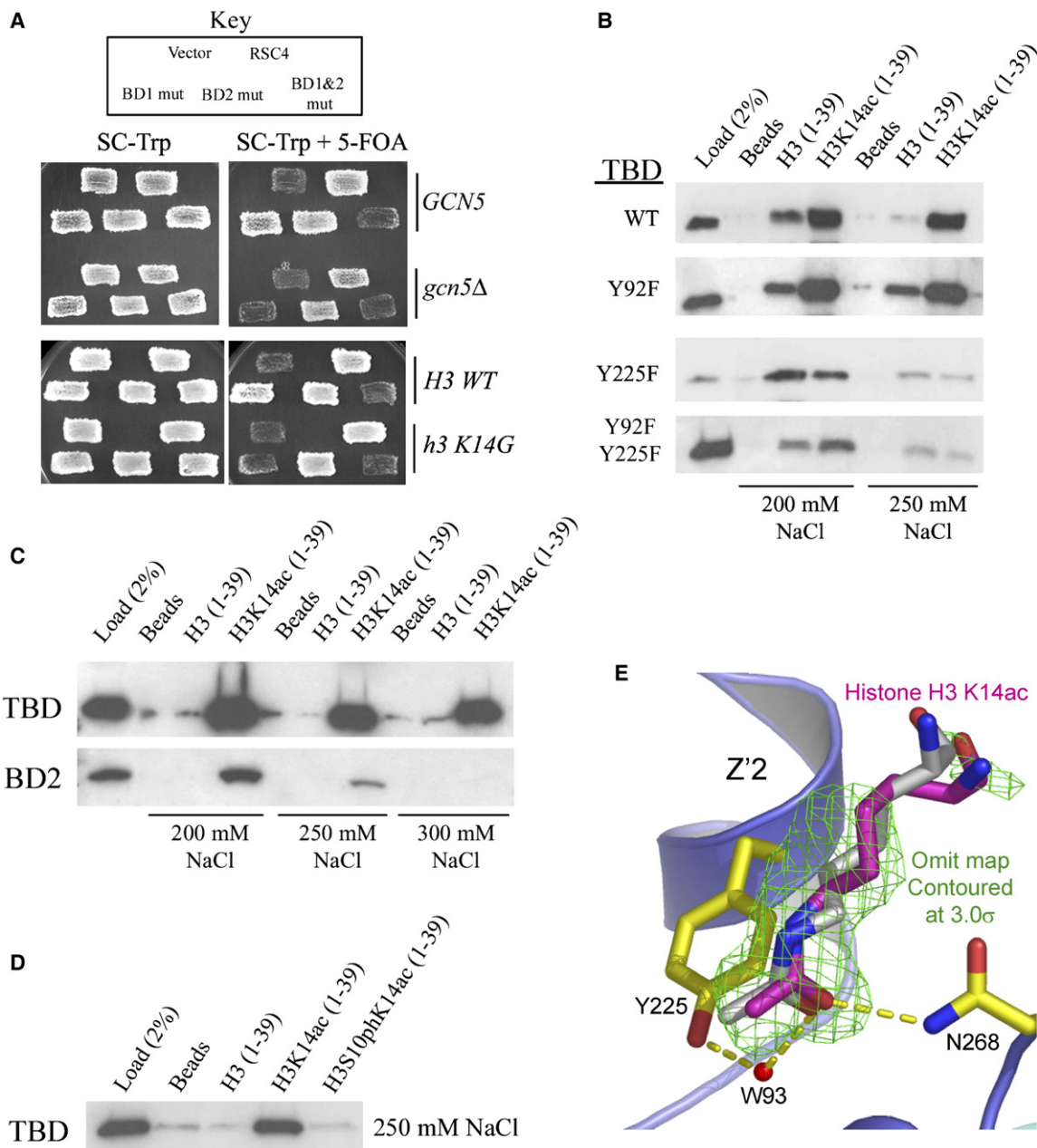
Figure 2. Rsc4 BD2 Interacts Genetically and Biochemically with Histone H3K14ac

(A) Complementation of *rsc4* BD mutants in WT (YBC627 and YBC2499), *gcn5Δ* (YBC2352), and histone *h3*K14G (YBC2501) strains. Patches were incubated for 2 days at 30°C. The *RSC4* construct location in the groups of five is provided by the key at top: vector, pRS314; RSC4, pRS314.*RSC4* (p1060); BD1 mutant, pRS314.*rsc4* Y92A Y93A (p1462); BD2 mutant, pRS314.*rsc4* Y225A Y226A (p1463); BD1&BD2 mutant, pRS314.*rsc4* Y92A Y93A Y225A Y226A (p1471). Strains were grown on selective media with or without 5-FOA, as 5-FOA enforces the loss of the pRS316.*RSC4* plasmid (right panels).

(B) Rsc4 BD2 is required for acetyl-specific binding to the H3K14 peptide. The binding of purified Rsc4(46–334) derivatives to biotinylated histone H3 tail peptides conjugated to streptavidin beads was examined by western blot. The H3 peptides extend from amino acid 1 to 39 of the H3 sequence and are either unmodified or acetylated at K14 as indicated. Binding avidity was further examined by increasing salt stringency in the wash buffers, as indicated. Western blots were probed with anti-Rsc4 polyclonal antibodies.

(C) Rsc4 BD2 is sufficient to bind to the H3K14ac peptide. Western blot analysis of purified Rsc4(36–321) TBD and Rsc4(157–321) BD2, as in (B).

(D) Binding by Rsc4 TBD and BD2 to H3K14ac is inhibited by H3S10ph. Western blot analysis of purified Rsc4 TBD bound to the H3 tail peptides, as in (B).

(E) Acetyl-lysine bound within the BD2 pocket of Rsc4(36–340) following soaking with H3(6–18) K14ac peptide. Difference density ($F_o − F_c$), contoured at 3.0 × rmsd, was phased on protein model refined prior to inclusion of the ligand. The closely overlapping acetyl lysine side chains from a Gcn5 bromo-domain:peptide complex structure (Owen et al., 2000) are shown colored white following superposition of the protein structures.

**Table 1. Data Collection and Refinement Statistics**

	Rsc4(36–340)	Rsc4(36–340)	Rsc4(1–321)	Rsc4(1–340)
		Histone (6–18, K14ac) Peptide Soak	Histone Chimera, Acetylated	Acetylated
Data Collection				
Space group	$R3_2$	$R3_2$	$C222_1$	$C2_1$
Cell dimensions (Å)	a = b = 95.9, c = 233.5	a = b = 95.0, c = 233.1	a = 86.1, b = 91.0, c = 263.2	a = 123.3, b = 83.2, c = 127.1, β = 109.3°
Resolution (Å)	20–1.80	50–1.75	50–2.20	50–2.35
Resolution Outer Shell (Å)	1.86–1.80	1.81–1.75	2.28–2.20	2.43–2.35
No. reflections	514,412	335,001	548,136	906,673
Unique reflections	37,132	39,000	49,197	50,527
R_{sym} (%)	5.5 (36.9)	6.8 (59.7)	7.8 (49.4)	7.6 (50.3)
$I/\sigma(I)$	25.5 (1.6)	33.7 (2.2)	32.0 (2.8)	26.9 (3.2)
Completeness (%)	96.2 (67.4)	94.6 (72.4)	95.3 (83.9)	99.5 (99.7)
Refinement				
R_{work}/R_{free} (%)	17.6/21.8	18.4/21.9	20.1/24.8	18.0/22.3
Number of Atoms				
Protein	2744	2669	5342	7790
Solvent	351	253	369	506
Average Isotropic B factor(Å)^2	30.6	34.2	51.4	40.7
Ramachandran Plot, Nonglycine Residue in				
Most favorable region (%)	92.1	91.7	91.4	91.7
Allowed region (%)	7.9	8.3	8.2	8.2
Rmsd				
Bond lengths (Å)	0.016	0.016	0.013	0.016
Bond angles (°)	1.241	1.406	1.416	1.211

outside of the primary binding pocket. Nevertheless, this structure supports the genetic and biochemical studies by showing that H3K14ac can bind Rsc4 BD2.

Rsc4 K25ac Binds BD1

In an effort to overcome the problem of low-affinity binding and to visualize a bound H3 peptide better, we took a chimera approach in which a very high local concentration of H3 peptide might be achieved by expressing the H3 tail as a fusion with the Rsc4 N terminus. The fusion included H3 residues 6–18, followed by eight residues containing a thrombin cleavage site, followed by Rsc4 residues 1–321 (Figure 1A). This construct contained the entire N-terminal sequence of Rsc4, whereas our initial crystal structures lacked the first 35 residues. The purified chimeric protein was acetylated at H3K14 using purified recombinant Gcn5, with progress of the reaction monitored by migration of the H3 peptide (following treatment and release with thrombin) using acid-urea gel electrophoresis. Acetylation was also monitored by western analysis, which revealed high levels of H3K14ac and very low levels of H3K9ac (data not shown). To more definitively identify

the acetylated lysines, we subjected tryptic fragments to mass spectrometric analysis. This revealed nearly complete acetylation at H3K14 and, surprisingly, nearly complete acetylation at Rsc4 K25. As described below, the modification of K25 was unexpected but highly fortuitous. The acetylated chimeric H3-Rsc4 protein was crystallized and the structure determined. Counter to the design goal, H3 residues were not ordered, and the BD2 pocket appeared to be empty. This was disappointing, but given the lack of information about likely binding orientation, the failure was not surprising. Remarkably, however, Rsc4 K25ac was present in the BD1 pocket, and the surrounding residues were well ordered, starting at residue 19 (Figure 3). An essentially identical arrangement was revealed in the subsequently determined crystal structure of Rsc4(1–340) bearing K25ac. This derivative bore its natural N terminus and lacked the H3 peptide, and quantitative acetylation at K25 (by Gcn5) was verified by mass spectrometry (data not shown). This binding could be recapitulated in *trans*, as a peptide containing Rsc4 residues 18–34 acetylated at K25 interacted with the TBD protein in vitro, though with low affinity (Figure S4).
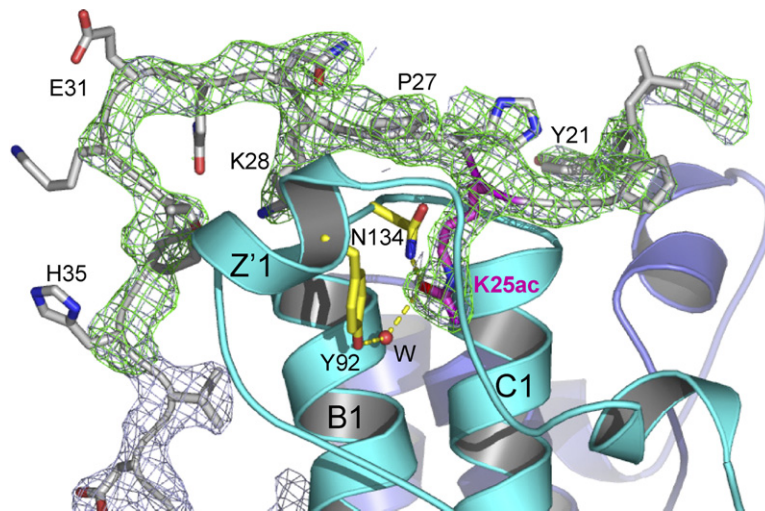
Figure 3. Binding of Rsc4 K25ac in BD1

Acetylated K25 binds BD1 and orders flanking residues. The $F_o - F_c$ map (3.0 × rmsd, green) and $2F_o - F_c$ map (1.2 × rmsd, gray) were phased from the protein model refined in the absence of residues 19–35. Residues involved in K25ac recognition are shown in yellow.
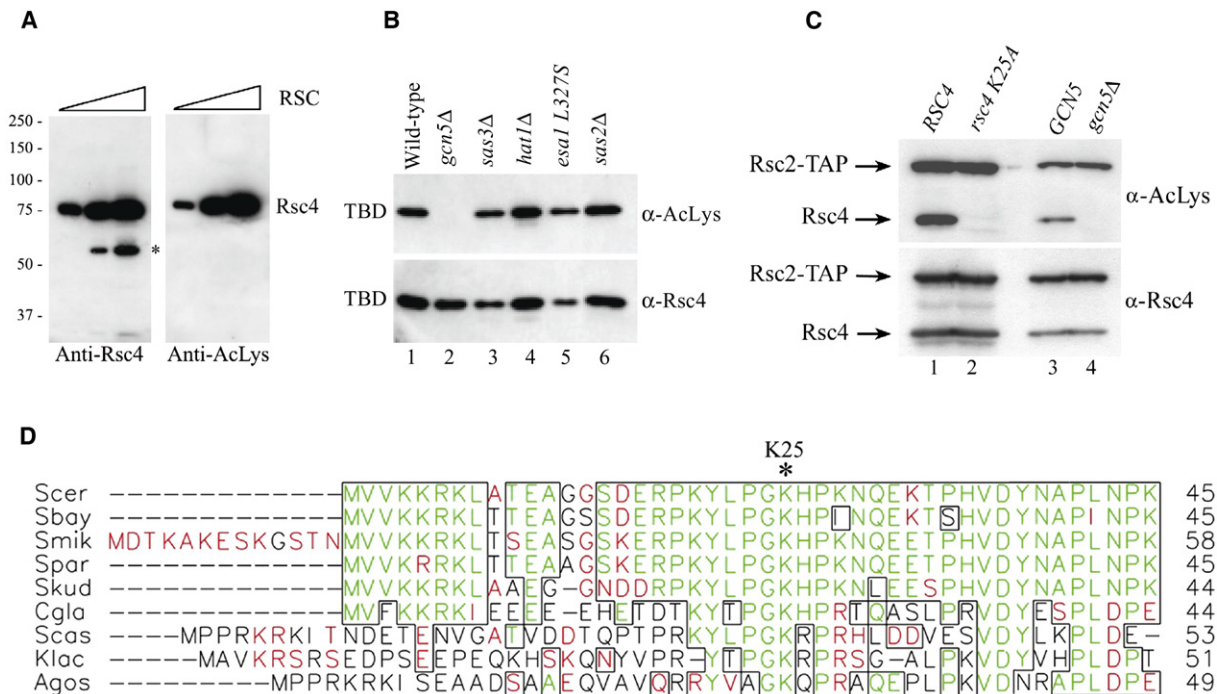
Rsc4 K25 Is Acetylated by Gcn5 In Vivo

Motivated by the surprising crystallographic observation that Rsc4 K25ac binds BD1, we sought to determine if this modification occurs in vivo. Western blot analysis of purified RSC complex using an antibody against acetyl-lysine revealed a single dominant band that comigrated with Rsc4 (Figure 4A). To identify the acetyltransferase that modifies Rsc4 in vivo, we expressed in yeast a Rsc4(1–340) construct that also included a nuclear targeting sequence and a 10 × HIS tag. We then purified this protein with nickel chelating chromatography and examined its acetylation state. Western analysis revealed clear acetylation in the WT strain and in a wide variety of strains lacking specific acetyltransferases. However, Rsc4 K25 acetylation was abolished in a strain lacking Gcn5 (Figure 4B). As a definitive test for the presence of Gcn5-dependent Rsc4 K25ac in the RSC complex in vivo, we made a Rsc4 derivative with a single amino acid replacement (K25A) as the sole source of Rsc4. This derivative or the WT Rsc4 was expressed in WT cells and purified as a component of the RSC complex using a TAP tag on the Rsc2 subunit (Figure 4C, lanes 1 and 2). Importantly, substitution of K25 abolished the acetylation of Rsc4 (Figure 4C, lanes 1 and 2). Furthermore, acetylation of WT Rsc4 present in the RSC complex was abolished when Rsc4 was isolated from a strain lacking Gcn5 (Figure 4C, lanes 3 and 4). The functional importance of K25 is supported by sequence alignment, which reveals that this lysine is highly conserved within yeast Rsc4 orthologs (Figure 4D). Moreover, G24 and P27 are also highly conserved, and the GKXP sequence matches the Gcn5 recognition motif determined from structural analysis of a Gcn5 HAT-histone H3 complex (Rojas et al., 1999).

Rsc4 K25 Is Important for Fitness and Gene Expression

To examine the in vivo consequences of Rsc4 K25 acetylation, we made a K25A mutation and assessed pheno-

types. The Rsc4 K25A mutation in isolation (and also K25R and K25Q) conferred only weak plate phenotypes, such as slightly slower growth on minimal medium under moderate heat stress (Figure S4). However, combining K25A with a conditional *rsc4* allele (*rsc4-2*, which has a point mutation in each bromodomain [Kasten et al., 2004]) greatly enhanced temperature sensitivity (Figure S4). This supports the proposal that acetylation of Rsc4 K25 contributes to RSC function in vivo. Subtle phenotypic effects can confer a fitness advantage that might be more clearly revealed in a growth competition assay. We therefore measured the fitness of the *rsc4* K25A mutant in direct competition with an isogenic WT strain and quantified gene fitness by the selection coefficient (*s*), which was obtained by comparing growth of the *rsc4* K25A mutant and the WT *RSC4* strain in coculture (Table 2). In this analysis, positive values of *s* indicate a selective disadvantage for the K25A mutant, while negative values of *s* indicate a greater selective advantage compared to WT. Surprisingly, under rich growth conditions (YPD, 30°C) the K25A mutant has a greater selective advantage ($s = -0.018$), indicating a 1.8% increase in the mutant K25A allele per generation in the coculture population under these conditions. In contrast, growth in minimal medium conditions (SD, 30°C) provides a selective advantage for the WT ($s = 0.021$), and this advantage is further increased ($s = 0.087$) when grown in minimal medium at elevated temperature (SD, 37°C). The loss of fitness for the K25A mutation when grown in minimal media conditions is highly significant ($p < 0.01$) and corresponds to an approximate 2.1% (30°C) or 8.7% (37°C) decrease in the K25A allele every generation.

We also examined the *rsc4* K25A mutant for changes in gene expression by performing transcriptional profiling from cells grown in minimal medium at slightly elevated temperature (33°C). In the K25A mutant, 80 genes were upregulated 2-fold or greater, and 61 genes were downregulated 2-fold or greater (Tables S1 and S2). Among the upregulated class, we did not observe a greater affect

Figure 4. Rsc4 K25 Is Acetylated In Vivo by Gcn5

(A) Rsc4 is acetylated in vivo. Increasing amounts of purified RSC complex (87.5, 350, and 1400 ng) were analyzed by western blot with anti-Rsc4 or anti-acetyl-lysine antibodies. An asterisk denotes a proteolytic fragment of Rsc4 that is evident when RSC is overloaded.

(B) Rsc4 is acetylated in vivo by Gcn5. Western blot analysis of partially purified (via nickel, NTA-Agarose) Rsc4(1–340) TBD (p2243) following expression in WT or various HAT mutant strains. Strains were the following: WT, (YBC1895); *gcn5Δ*, (YBC1662); *sas3Δ*, (YBC1911); *hat1Δ*, (YBC2493); *esa1* L327S, (LPY3430); and *sas2Δ*, (YBC1857).

(C) Rsc4 resident in RSC complex is acetylated at K25 by Gcn5 in vivo. Western blot analysis of partially purified RSC isolated via the Rsc2-TAP tag from strains bearing either *RSC4* or the *rsc4 K25A* mutant or *GCN5* or *gcn5Δ*. The protein A portion of the TAP tag (not cleaved in this procedure) serves as an internal control, as it is recognized by all antibodies, including anti-acetyl-lysine or anti-Rsc4. Strains included the following: *RSC4*, (YBC2814); *rsc4* K25A, (YBC2815); *GCN5*, (YBC2825); *gcn5Δ*, (YBC2822).

(D) Alignment of the amino termini of Rsc4 orthologs from various yeast species (Clustal W). Identical amino acids are shown in green, and similar amino acid residues are shown in red, with regions of high similarity blocked together (PrettyPlot). Rsc4 K25, asterisk at top. Species include the following: *S. cerevisiae* (Scer), *S. bayanus* (Sbay), *S. mikatae* (Smik), *S. paradoxus* (Spar), *S. kudrievzevii* (Skud), *C. glabrata* (Cgla), *S. castellii* (Scas), *K. lactis* (Klac), and *A. gossypii* (Agos).

on genes of a particular inherent transcriptional frequency. Common classes of upregulated genes include those involved in cell wall integrity, those involved in the response to cell stress, and those encoding proteins that reside in the cell membrane. Misregulation of genes involved in cell wall integrity has been observed with other *rsc* mutants, including conditional *rsc4* alleles (Angus-Hill et al., 2001; Kasten et al., 2004). Taken together, our genetic

Table 2. Competition of the *rsc4 K25A* Strain against Wild-Type

Media	s	Impact[a]	n	Number of Cultures	p
YPD 30°C	−0.018 ± 0.0036	1.8%	6	7	<0.01
SD 30°C	0.021 ± 0.0069	−2.1%	6	8	<0.01
SD 37°C	0.087 ± 0.0059	−8.7%	6	4	<0.01

Media are described in the Experimental Procedures section. Selection coefficients (s) ± the standard deviation for *rsc4 K25A* relative to the WT strain were measured as described in the Experimental Procedures section. A positive value for s indicates a greater selective advantage for the WT strain, and a negative value indicates that the mutant has a greater selective advantage. Indicated are the number of time points (n) at which genotype frequencies were measured and the number of cultures analyzed for each growth condition. The statistical significance (p) for a test of the null hypothesis that the selection coefficient is not different from zero was determined.
[a] Impact indicates the approximate percent change in the mutant allele relative to the WT allele per generation in coculture.
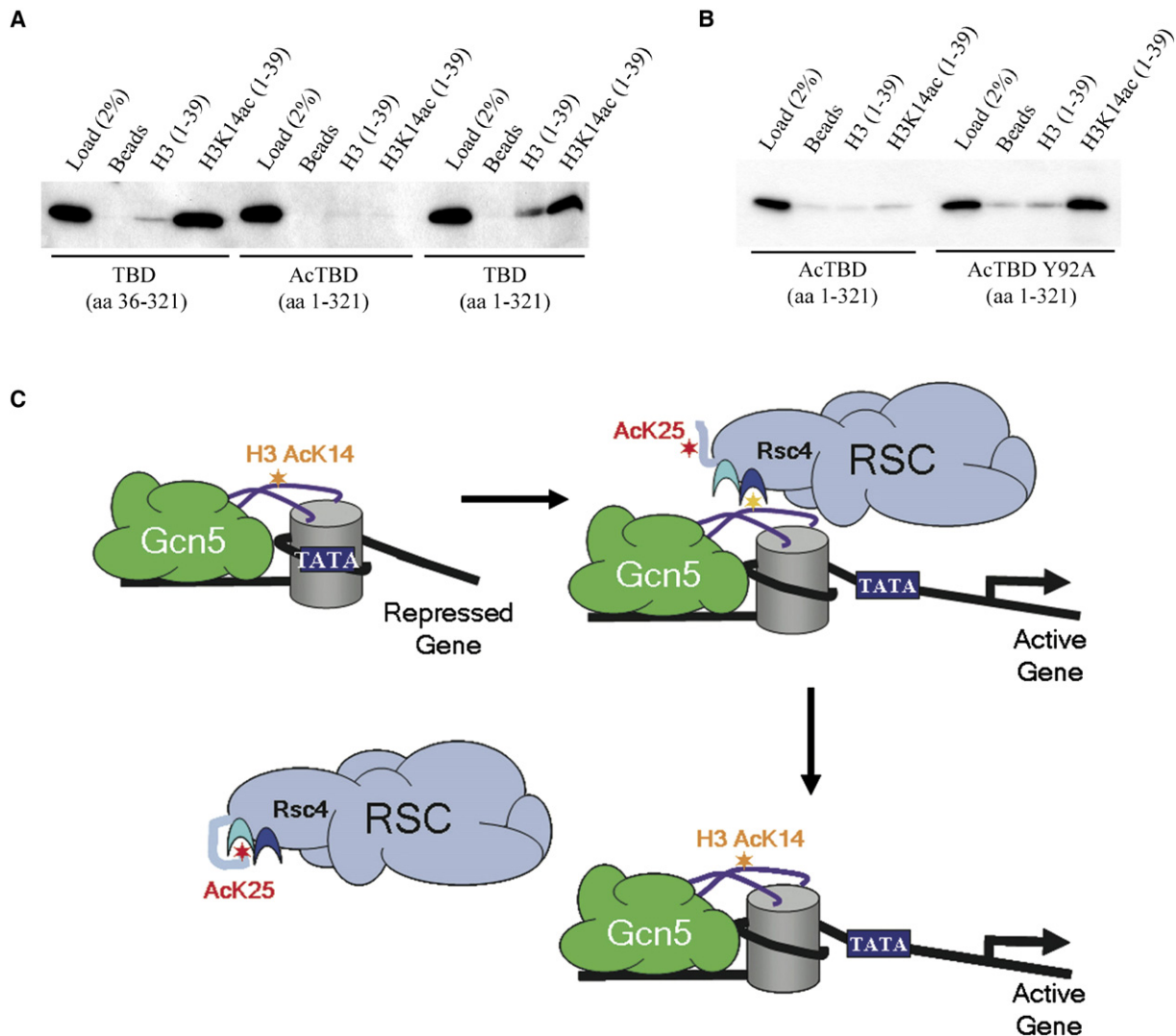
Figure 5. Inhibition of H3K14ac Binding Involves Rsc4 K25ac Binding to BD1

(A) Rsc4 K25 acetylation inhibits H3K14ac binding. Binding of purified nonacetylated and acetylated TBD to biotinylated histone H3 tail peptides conjugated to streptavidin beads was examined by western analysis. Rsc4(36–321) TBD was expressed from p1617 and Rsc4(1–321) TBD was expressed from p1616. Rsc4(1–321) TBD was acetylated by Gcn5 where indicated, and acetylation at K25 was confirmed by mass spectrometry analysis (data not shown). Binding and wash buffers contained 100 mM NaCl.

(B) Western blot analysis of purified WT and mutant acetylated Rsc4(1–321) TBD bound to H3 peptides. Bead bindings and washes were conducted at 150 mM NaCl. Rsc4 K25ac(1–321) TBD was expressed from p1617 and Rsc4 K25Ac(1–321) Y92A TBD was expressed from p2296. Proteins were acetylated by Gcn5, and acetylation was confirmed by mass spectrometry analysis (data not shown).

(C) Model for Rsc4 autoregulation. Gcn5 acetylation of H3K14 facilitates Rsc4 interaction with H3K14ac and also the subsequent release of Rsc4 from chromatin by acetylating Rsc4 K25, which binds in BD1 and antagonizes Rsc4 binding to H3K14ac.

analysis, fitness determination, and gene profiling analysis demonstrate a significant role for Rsc4 K25 in RSC function in vivo.

Rsc4 K25ac Binding to BD1 Inhibits H3K14ac Binding to BD2

Having demonstrated that Rsc4 K25 is acetylated by Gcn5 both in vitro and in vivo, we investigated possible mechanistic roles for this modification. In principle, the binding of K25ac in BD1 could have a positive, neutral,

or negative impact on H3K14ac binding to BD2. To test this, we applied the histone tail peptide binding assay utilized above and prepared both K25-acetylated and nonacetylated versions of Rsc4(1–321). The results show that K25 acetylation of Rsc4(1–321) significantly inhibited binding of H3K14ac peptides to BD2 (Figure 5A). The importance of K25ac binding to BD1 for this inhibition was tested more precisely by using Rsc4(1–321) Y92A protein, which is crippled for binding to BD1. Importantly, binding to H3K14ac peptides is largely restored in the Y92A

derivative, thereby indicating that binding of K25ac to BD1 is coupled with inhibition of H3K14ac binding to BD2 (Figure 5B). The mechanism for this inhibition is not immediately obvious, because BD1 and BD2 are separated by 20 Å. Our preferred model is that N-terminal residues that become ordered upon binding of K25ac to BD1 overlap the site of H3 residues that bind cooperatively with the K14ac - BD2 interaction, although an allosteric propagation of a subtle conformational change is also possible.

Models for Biological Mechanism

Our structural, biochemical, and genetic data have established that H3K14ac binds Rsc4 BD2 and that additional interactions with flanking residues in the H3 tail (not resolved in the structure) also contribute to binding affinity. The interaction is inherently weak, but it is specific and biologically important, and binding in the biological context is presumably enhanced by cooperative effects involving the additional DNA- and nucleosome-interacting domains, such as the SWIRM, SANT, and additional bromodomains of RSC subunits (Boyer et al., 2002; Da et al., 2006; Yu et al., 2003). Weak interactions are appropriate components of such regulatory switches, because they are reversible and avoid saturation with incorrect binding partners, such as other acetylated lysine residues. Our surprising finding that Rsc4 K25 is acetylated by Gcn5 both in vitro and in vivo reveals that yeast Gcn5 is both a HAT and a protein acetyltransferase. This is consistent with the roles of related enzymes such as PCAF and p300 in vertebrates (Gu and Roeder, 1997; Mujtaba et al., 2002). Also surprising was our discovery that acetylated Rsc4 K25 bound to BD1. The biological relevance of the interaction is indicated by our growth competition and transcriptional profiling data. The magnitude of the selection coefficients obtained shows that prolonged stress conditions such as those examined would cause the loss of the mutant population (8.7% loss per generation). The likely mechanistic basis for the biological loss of fitness is our finding that this interaction inhibits binding of H3K14ac peptides to BD2. Another direction that merits future study is that BD1 and/or BD2 likely has additional binding partners; these bromodomains are essential for viability, whereas their currently identified ligands are not. To find them, we have tried many other histone tail peptide substrates in our in vitro binding assays, including H3 K9ac, H3 K23ac, H3 K9ac K18ac, and H3 K18ac K27ac in addition to the series tested previously (Kasten et al., 2004). However, none of these provided acetyl-enhanced binding. In principle, the binding of Rsc4 TBDs to alternative ligands might be regulated by the mechanisms revealed here. For example, the binding of Rsc4 K25ac to BD1 might enhance the binding of another ligand to BD2. Alternatively, BD1 may bind an alternative ligand on a histone tail when K25 is not acetylated, leaving the BD1 pocket available and perhaps enabling cooperativity with H3K14ac bound in BD2.

Gcn5 acetylates ligands for both BD1 and BD2, and these ligands compete for binding to Rsc4. This raises the possibility that Gcn5 activity serves as a switch; Gcn5 acetylation of H3K14 would favor RSC-nucleosome binding, and this interaction would be countered by acetylation of Rsc4 K25. One attractive possibility is that this mechanism regulates the residence time of RSC to sites of remodeling (Figure 5C). In this model, activators recruit Gcn5 to promoter regions where it acetylates H3K14. This recruits RSC to promote nucleosome sliding and enhance promoter accessibility and also places Rsc4 in the vicinity of Gcn5, which then acetylates K25 and triggers release of RSC from the now-remodeled nucleosome. Finally, autoregulatory mechanisms, in which a binding protein or enzyme adopts a repressed conformation in response to intramolecular binding of a posttranslationally attached group, have been extensively characterized for kinases (reviewed in Kuriyan and Cowburn, 1997) and recently described for ubiquitylation (Hoeller et al., 2006). Our demonstration that RSC function is optimized by an analogous approach raises the possibility that mechanisms of this type might be widespread for acetylation and other modifications associated with chromatin dynamics.

EXPERIMENTAL PROCEDURES

See the Supplemental Data for details of media, strain lists, plasmid lists, protein expression and purification, in vitro acetylation, and crystallographic methods.

Histone Tail Binding Assay

Biotinylated histone tail peptides were bound to streptavidin beads (Invitrogen) as previously described (Kasten et al., 2004) and resuspended in a 50% slurry. Binding assays were conducted by rotating 15 μl of the peptide/bead slurry (20 nmol peptide/100 μl bed volume beads) with 500 ng purified Rsc4 protein in peptide binding buffer (PBB) (20 mM Tris [pH 7.5], 150 mM NaCl, 5% glycerol, 0.05% Tween-20, 1 mM EDTA, 1 mM β-mercaptoethanol, protease inhibitors) at 4°C for 3 hr. Typically, the beads were washed twice with PBB and twice with PBB containing 250 mM NaCl or the alternative NaCl concentrations indicated, followed by elution with 4 × SDS sample buffer.

RSC Purification, Extract Preparation, Immunoprecipitation, and Antibodies

RSC was purified as previously described (Saha et al., 2002). Whole-cell extracts were prepared as previously described (Cairns et al., 1999). Partially purified RSC was analyzed for Rsc4 acetylation in the gcn5Δ and rsc4 K25A mutant and was derived from whole-cell extracts lysed in 3 × lysis buffer (60 mM HEPES [pH 7.6], 30% glycerol, 750 mM NaCl, 0.3% Tween-20, 30 mM EDTA, 1.5 mM DTT, protease inhibitors), which were then bound to IgG beads, washed three times with IPP150 (20 mM HEPES [pH 7.6], 10% glycerol, 150 mM NaCl, 0.1% Tween-20, 10 mM EDTA, 0.5 mM DTT, protease inhibitors), and eluted by boiling in 4 × SDS sample buffer prior to western blot analysis. The anti-Rsc4 antibody was made to the full-length protein and was previously described (Kasten et al., 2004). The anti-acetyl lysine antibody was from Cell Signaling.

Affinity Purification of Rsc4(1–340) from Yeast

Rsc4(1–340) preceded by 10 × HIS and 2 × NLS sequences expressed in yeast was nickel affinity purified prior to examining acetylation. Whole-cell extracts were prepared as previously described (Saha et al., 2005) except in modified breaking buffer (12% glycerol, 50 mM Tris [pH 7.5], 0.1% Triton X-100, 500 mM NaCl, 1.5 mM β-mercaptoethanol, protease inhibitors). Extracts (3 mg) were incubated with

100 μl bed volume of Ni-NTA agarose (QIAGEN) for 3 hr at 4°C, poured into a small column, washed three times (1.2 ml) with wash buffer (50 mM NaPhosphate [pH 8.0], 150 mM NaCl, 10% glycerol) containing increasing amounts of imidazole (from 10 mM to 40 mM). Bound protein was eluted with wash buffer containing 300 mM imidazole and protease inhibitors prior to western blot analysis.

rsc4 K25A Fitness Determination

Fitness determinations compared isogenic strains, differing only at *rsc4* K25A mutation, which were prepared by standard yeast gene transplacement methods. Comparisons used a method based on (Thatcher et al., 1998). Competition cocultures were established by inoculating 2 ml of YPD (rich media) or SD supplemented as needed for auxotrophies (minimal media) with 32 μl each from overnight cultures of YBC2898 and YBC2899 grown in YPD or SD. Equal numbers of cells (by OD reading) from each strain were inoculated, and cultures were incubated at 30°C or 37°C and were back diluted into fresh media daily. Each day, 1 ml of the competition coculture was collected and used to prepare genomic DNA using the YeaStar Genomic DNA kit (Zymo Research). Quantitative PCR (qPCR) was utilized to determine *RSC4* genotype frequencies. Primers were designed so that the 3′ ends recognize either the K25 or the K25A codon allowing these primers to differentiate between the two *RSC4* alleles. Genomic DNA harvested periodically from the competition cocultures was used in separate qPCR procedures essentially as previously described (Roberts et al., 2003) to determine the quantity of each allele individually. Primer for *RSC4* K25 detection was the following: (BC3550) GCCTAAATACTTGCCGGGAAAA. Primer for *rsc4* K25A detection was the following: (BC3551) CTAAATACTTGCCGGGAGCC. *RSC4* reverse primer used for detection of either allele was the following: (BC3539) TGTATTTGTCGATAAGAACATCCAAAGTG. The average of three PCR replicates was taken for each genomic DNA analyzed. The change in allele ratio with time is given by the equation $\ln(R_t) = \ln(R_0) - st$ (where R_0 is the initial genotype ratio, R_t is the ratio after t generations, and s is the selection coefficient) (Thatcher et al., 1998). The selection coefficient for the *rsc4* K25A mutant relative to WT in each growth condition was calculated by fitting the above equation to the qPCR frequency data.

Supplemental Data

Supplemental Data include Supplemental Experimental Procedures, four figures, four tables, and Supplemental References and can be found with this article online at http://www.molecule.org/cgi/content/full/27/5/817/DC1/.

REFERENCES

Angus-Hill, M.L., Schlichter, A., Roberts, D., Erdjument-Bromage, H., Tempst, P., and Cairns, B.R. (2001). A Rsc3/Rsc30 zinc cluster dimer reveals novel roles for the chromatin remodeler RSC in gene expression and cell cycle control. Mol. Cell 7, 741–751.

Baetz, K.K., Krogan, N.J., Emili, A., Greenblatt, J., and Hieter, P. (2004). The ctf13–30/CTF13 genomic haploinsufficiency modifier screen identifies the yeast chromatin remodeling complex RSC, which is required for the establishment of sister chromatid cohesion. Mol. Cell. Biol. 24, 1232–1244.

Boyer, L.A., Langer, M.R., Crowley, K.A., Tan, S., Denu, J.M., and Peterson, C.L. (2002). Essential role for the SANT domain in the functioning of multiple chromatin remodeling enzymes. Mol. Cell 10, 935–942.

Brownell, J.E., Zhou, J., Ranalli, T., Kobayashi, R., Edmondson, D.G., Roth, S.Y., and Allis, C.D. (1996). Tetrahymena histone acetyltransferase A: a homolog to yeast Gcn5p linking histone acetylation to gene activation. Cell 84, 843–851.

Cairns, B.R. (2005). Chromatin remodeling complexes: strength in diversity, precision through specialization. Curr. Opin. Genet. Dev. 15, 185–190.

Cairns, B.R., Lorch, Y., Li, Y., Zhang, M., Lacomis, L., Erdjument-Bromage, H., Tempst, P., Du, J., Laurent, B., and Kornberg, R.D. (1996). RSC, an essential, abundant chromatin-remodeling complex. Cell 87, 1249–1260.

Cairns, B.R., Schlichter, A., Erdjument-Bromage, H., Tempst, P., Kornberg, R.D., and Winston, F. (1999). Two functionally distinct forms of the RSC nucleosome-remodeling complex, containing essential AT hook, BAH, and bromodomains. Mol. Cell 4, 715–723.

Carey, M., Li, B., and Workman, J.L. (2006). RSC exploits histone acetylation to abrogate the nucleosomal block to RNA polymerase II elongation. Mol. Cell 24, 481–487.

Chai, B., Huang, J., Cairns, B.R., and Laurent, B.C. (2005). Distinct roles for the RSC and Swi/Snf ATP-dependent chromatin remodelers in DNA double-strand break repair. Genes Dev. 19, 1656–1661.

Chang, C.R., Wu, C.S., Hom, Y., and Gartenberg, M.R. (2005). Targeting of cohesin by transcriptionally silent chromatin. Genes Dev. 19, 3031–3042.

Da, G., Lenkart, J., Zhao, K., Shiekhattar, R., Cairns, B.R., and Marmorstein, R. (2006). Structure and function of the SWIRM domain, a conserved protein module found in chromatin regulatory complexes. Proc. Natl. Acad. Sci. USA 103, 2057–2062.

Fischle, W., Wang, Y., Jacobs, S.A., Kim, Y., Allis, C.D., and Khorasanizadeh, S. (2003). Molecular basis for the discrimination of repressive methyl-lysine marks in histone H3 by Polycomb and HP1 chromodomains. Genes Dev. 17, 1870–1881.

Gu, W., and Roeder, R.G. (1997). Activation of p53 sequence-specific DNA binding by acetylation of the p53 C-terminal domain. Cell 90, 595–606.

Hassan, A.H., Prochasson, P., Neely, K.E., Galasinski, S.C., Chandy, M., Carrozza, M.J., and Workman, J.L. (2002). Function and selectivity of bromodomains in anchoring chromatin-modifying complexes to promoter nucleosomes. Cell 111, 369–379.

Hassan, A.H., Awad, S., and Prochasson, P. (2006). The Swi2/Snf2 bromodomain is required for the displacement of SAGA and the octamer transfer of SAGA-acetylated nucleosomes. J. Biol. Chem. 281, 18126–18134.

Hoeller, D., Crosetto, N., Blagoev, B., Raiborg, C., Tikkanen, R., Wagner, S., Kowanetz, K., Breitling, R., Mann, M., Stenmark, H., and Dikic, I. (2006). Regulation of ubiquitin-binding proteins by monoubiquitination. Nat. Cell Biol. 8, 163–169.

Howe, L., Auston, D., Grant, P., John, S., Cook, R.G., Workman, J.L., and Pillus, L. (2001). Histone H3 specific acetyltransferases are essential for cell cycle progression. Genes Dev. 15, 3144–3154.

Hudson, B.P., Martinez-Yamout, M.A., Dyson, H.J., and Wright, P.E. (2000). Solution structure and acetyl-lysine binding activity of the GCN5 bromodomain. J. Mol. Biol. 304, 355–370.

Jacobson, R.H., Ladurner, A.G., King, D.S., and Tjian, R. (2000). Structure and function of a human TAFII250 double bromodomain module. Science 288, 1422–1425.

Kasten, M., Szerlong, H., Erdjument-Bromage, H., Tempst, P., Werner, M., and Cairns, B.R. (2004). Tandem bromodomains in the chromatin remodeler RSC recognize acetylated histone H3 Lys14. EMBO J. 23, 1348–1359.

Kornberg, R.D., and Lorch, Y. (1999). Twenty-five years of the nucleosome, fundamental particle of the eukaryote chromosome. Cell 98, 285–294.

Kouzarides, T. (2000). Acetylation: a regulatory modification to rival phosphorylation? EMBO J. 19, 1176–1179.

Kuriyan, J., and Cowburn, D. (1997). Modular peptide recognition domains in eukaryotic signaling. Annu. Rev. Biophys. Biomol. Struct. 26, 259–288.

Lo, W.S., Trievel, R.C., Rojas, J.R., Duggan, L., Hsu, J.Y., Allis, C.D., Marmorstein, R., and Berger, S.L. (2000). Phosphorylation of serine 10 in histone H3 is functionally linked in vitro and in vivo to Gcn5-mediated acetylation at lysine 14. Mol. Cell 5, 917–926.

Mujtaba, S., He, Y., Zeng, L., Farooq, A., Carlson, J.E., Ott, M., Verdin, E., and Zhou, M.M. (2002). Structural basis of lysine-acetylated HIV-1 Tat recognition by PCAF bromodomain. Mol. Cell 9, 575–586.

Owen, D.J., Ornaghi, P., Yang, J.C., Lowe, N., Evans, P.R., Ballario, P., Neuhaus, D., Fileteci, P., and Travers, A.A. (2000). The structural basis for the recognition of acetylated histone H4 by the bromodomain of histone acetyltransferase gcn5p. EMBO J. 19, 6141–6149.

Roberts, D.N., Stewart, A.J., Huff, J.T., and Cairns, B.R. (2003). The RNA polymerase III transcriptome revealed by genome-wide localization and activity-occupancy relationships. Proc. Natl. Acad. Sci. USA 100, 14695–14700.

Rojas, J.R., Trievel, R.C., Zhou, J., Mo, Y., Li, X., Berger, S.L., Allis, C.D., and Marmorstein, R. (1999). Structure of Tetrahymena GCN5 bound to coenzyme A and a histone H3 peptide. Nature 401, 93–98.

Saha, A., Wittmeyer, J., and Cairns, B.R. (2002). Chromatin remodeling by RSC involves ATP-dependent DNA translocation. Genes Dev. 16, 2120–2134.

Saha, A., Wittmeyer, J., and Cairns, B.R. (2005). Chromatin remodeling through directional DNA translocation from an internal nucleosomal site. Nat. Struct. Mol. Biol. 12, 747–755.

Shen, W., Xu, C., Huang, W., Zhang, J., Carlson, J.E., Tu, X., Wu, J., and Shi, Y. (2007). Solution structure of human Brg1 bromodomain and its specific binding to acetylated histone tails. Biochemistry 46, 2100–2110.

Soutourina, J., Bordas-Le Floch, V., Gendrel, G., Flores, A., Ducrot, C., Dumay-Odelot, H., Soularue, P., Navarro, F., Cairns, B.R., Lefebvre, O., and Werner, M. (2006). Rsc4 connects the chromatin remodeler RSC to RNA polymerases. Mol. Cell. Biol. 26, 4920–4933.

Strahl, B.D., and Allis, C.D. (2000). The language of covalent histone modifications. Nature 403, 41–45.

Sun, H., Liu, J., Zhang, J., Shen, W., Huang, H., Xu, C., Dai, H., Wu, J., and Shi, Y. (2007). Solution structure of BRD7 bromodomain and its interaction with acetylated peptides from histone H3 and H4. Biochem. Biophys. Res. Commun. 358, 435–441. Published online May 2, 2007. 10.1016/j.bbrc.2007.04.139.

Syntichaki, P., Topalidou, I., and Thireos, G. (2000). The Gcn5 bromodomain co-ordinates nucleosome remodelling. Nature 404, 414–417.

Thatcher, J.W., Shaw, J.M., and Dickinson, W.J. (1998). Marginal fitness contributions of nonessential genes in yeast. Proc. Natl. Acad. Sci. USA 95, 253–257.

Trievel, R.C., Rojas, J.R., Sterner, D.E., Venkataramani, R.N., Wang, L., Zhou, J., Allis, C.D., Berger, S.L., and Marmorstein, R. (1999). Crystal structure and mechanism of histone acetylation of the yeast GCN5 transcriptional coactivator. Proc. Natl. Acad. Sci. USA 96, 8931–8936.

Yu, J., Li, Y., Ishizuka, T., Guenther, M.G., and Lazar, M.A. (2003). A SANT motif in the SMRT corepressor interprets the histone code and promotes histone deacetylation. EMBO J. 22, 3403–3410.

Yukawa, M., Katoh, S., Miyakawa, T., and Tsuchiya, E. (1999). Nps1/Sth1p, a component of an essential chromatin-remodeling complex of Saccharomyces cerevisiae, is required for the maximal expression of early meiotic genes. Genes Cells 4, 99–110.

Accession Numbers

Protein Data Bank entry codes are 2R0S for Rsc4(36–340), 2R0Y for Rsc4(36–340) peptide soak, 2R0V for acetylated Rsc4(1–340), and 2R1O for acetylated histone-Rsc4(1–321) chimera.

Supplemental Data

Autoregulation of the Rsc4 Tandem

Bromodomain by Gcn5 Acetylation

Andrew P. VanDemark, Margaret M. Kasten, Elliott Ferris, Annie Heroux, Christopher P. Hill, and Bradley R. Cairns

Supplemental Experimental Procedures

Media, strains, plasmids

Standard procedures were used for media preparation, transformations, integrations, sporulations, and tetrad analysis. All strains are derivatives of S288C. Strain genotypes are listed in Table S3. Yeast Rsc4 constructs were obtained from genomic DNA by PCR. The H3-Rsc4(1-321) chimera was generated by PCR utilizing primers containing sequence for histone H3 (residues 6-18) followed by a thrombin protease recognition site with short linkers separating the thrombin site from both the histone and Rsc4 sequence. Details of other plasmid constructions are available upon request. All plasmid constructs generated through PCR were sequence verified. Plasmids bearing site-directed mutations in *RSC4* or histone H3 were prepared using the QuikChange method (Stratagene), subcloned, and fully sequenced. The pET151/D-TOPO vector used to express the recombinant Rsc4 proteins is from Invitrogen and results in fusion proteins that bear a 6xHis tag followed by the V5 epitope and a TEV recognition site at the amino terminus of the protein. Plasmids are listed in Table S4.

Protein expression and purification

Wild type and mutant recombinant Rsc4(46-334) used in the binding assays in Figure 2B were expressed fused to N-terminal Flag and C-terminal 10xHis tags, and purified using standard methods. The purified proteins were analyzed or further purified by size exclusion chromatography on a Superdex 200 column (GE Healthcare).

All other Rsc4 constructs were expressed in *E.coli* Codon+ (RIL) cells (Stratagene) as His-tagged fusions using a pET151/D-TOPO cloning/expression plasmid (Invitrogen). Cells were grown in ZY autoinduction media (Studier, 2005) at room temperature for 24-30 hours, harvested by centrifugation, and lysed by sonication in 25 mM HEPES (pH 7.5), 500 mM NaCl, 5% glycerol, 10 mM imidazole, 0.5 mM β-mercaptoethanol. Rsc4 proteins were purified by nickel affinity chromatography (Qiagen), followed by an overnight digestion at room temperature with TEV protease in a dialysis bag against a buffer containing 20 mM HEPES (pH 8.0), 500 mM NaCl, 5% glycerol, and 0.5 mM β-mercaptoethanol. A second round of nickel affinity chromatography was used to remove any uncleaved protein and the His-tagged TEV protease. Gel filtration and buffer transfer was performed on a Superdex-200 column (GE Healthcare) in 20 mM Tris-HCl (pH 7.5), 150 mM NaCl, 2% glycerol, and 0.5 mM DTT, with peak fractions eluting as an apparent monomer. Protein was concentrated to 15 mg/ml and stored at 4ºC, where it was stable for many months. Selenomethionine-substituted Rsc4(36-340) was expressed (Van Duyne et al., 1993) and purified using the same protocol as native protein, with the

addition of 5mM β-mercaptoethanol in the lysis and TEV cleavage buffers.

Gcn5 was expressed using a pET11a bacterial expression vector as a 7x N-terminal His-tagged fusion. Gcn5 was expressed in *E.coli* using IPTG induction, lysed in 25mM HEPES (pH 7.5), 500 mM NaCl, 5% glycerol, and 1 mM β-mercaptoethanol, and purified via nickel chelating and gel filtration chromatography. Peak fractions were collected and dialyzed into 20 mM HEPES (pH 7.5), 200mM NaCl, and 50% glycerol, and stored at –80°C.

In vitro acetylation reactions

Purified Rsc4(1-340) or H3-Rsc4(1-321) proteins were concentrated to 15 mg/ml and acetylated in 20mM Tris (pH 7.5), 150 mM NaCl, 5% glycerol, 0.5 mM DTT, and 5 mM acetyl-CoA, and 1.0 mg/ml Gcn5. The reaction was carried out at 30°C for 60-90 minutes. Following acetylation, nickel affinity chromatography was used to remove the Gcn5 followed by gel filtration using a Superdex-200 column (in 20 mM HEPES [pH 7.5], 100 mM NaCl, 2% glycerol, and 0.5 mM DTT) to remove the excess acetyl-CoA. Notably, the non-acetylated Rsc4 protein control was subjected to all the same procedures and components, with omission of Ac-CoA from the reaction, and acetylation specificity was confirmed by mass spectrometric analysis.

The efficiency of histone acetylation was monitored by cleaving a small amount with thrombin to release the histone portion of the chimera, followed by electrophoresis on a 15% acid-urea gel (Hirose, 1988). Acetylation at Rsc4-K25 was identified by mass

spectrometry of proteolytic digested protein using nanoelectrospray with a LTQ-FT mass spectrometer (ThermoElectron). Samples were introduced on a 75 μm ID x 10 cm column (C18) at 400 nl/min with an acetonitrile gradient (in 0.1% formic acid). Primary data were acquired in the FT part of the instrument (with less than 2 ppm mass error) and MS/MS/ data were acquired in LTQ (linear-ion-trap) part of the instrument. Database searches were performed with Mascot. Subsequent analysis of non-proteolyzed fragments by electrospray ionization mass spectrometry was performed using a Quattro-II (Micromass). After C18 ziptip desalting, the sample was introduced by infusion at 3 μl/min. Data were processed into molecular mass spectra with MaxEnt software (Micromass). These data revealed that the product was overwhelmingly a doubly acetylated protein for the Rsc4:Histone chimera and a singly acetylated protein when the Rsc4(1-340) protein is used.

Crystallization

Prior to crystallization, purified proteins were concentrated to 15 mg/ml in the gel filtration buffer using a Vivaspin concentrator (Millipore). All crystals were grown by vapor diffusion with the drop containing one part protein solution mixed with one part reservoir. Rsc4(36-340) crystals grew overnight against a reservoir solution of 0.1M phosphate-citrate (pH 4.2), 0.2 M NaCl, 0.2 M ammonium sulfate, 20% PEG 3000, and 5% glycerol. Single crystals were moved into a cryoprotection solution composed of the reservoir condition made up with 15-20% glycerol and flash frozen using liquid nitrogen. Crystals of Rsc4(36-340):H3 complex were obtained by soaking Rsc4(36-340) crystals in a high (~40 mM) concentration of histone H3 peptide (6-18, K14ac) overnight at 4°C.

Following peptide soak, the crystals were transferred briefly (few seconds) into cryoprotectant and flash frozen.

Crystals of the acetylated H3-Rsc4 chimera grew over a period of 3 weeks using a reservoir condition containing 0.1 M Tris-HCl (pH8.5), 0.2 M lithium sulfate, and 28-30% PEG 3000. Single crystals were cryoprotected by increasing the glycerol concentration to 15-20% in 2.5% intervals and flash freezing with liquid nitrogen. Crystals of acetylated Rsc4(1-340) were grown overnight using a reservoir of 0.1 M Tris-HCl (pH 8.0), 0.2 M ammonium sulfate, and 22% PEG 4000. Single crystals were moved into a cryoprotection solution composed of the reservoir condition made up with 20% glycerol and flash frozen using liquid nitrogen.

Structure Determinations

SAD data were collected to 3.0 Å resolution from a crystal of selenomethionine-substituted Rsc4(36-340) and processed with HKL2000. SOLVE (Terwilliger and Berendzen, 1999) located six Se sites and generated a readily interpretable map. Initial model building was performed by RESOLVE, followed by manual model building in Xfit (McRee, 1999). High resolution data on Rsc4(36-340) was collected in house using an RAXIS-IV detector (Rigaku) and processed with DENZO and SCALEPACK (Otwinowski and Minor, 1997). All other data were collected at NSLS beamline X26-C and processed with HKL2000 (Otwinowski and Minor, 1997). Structures of acetylated Rsc4 constructs were determined by molecular replacement using PHASER (McCoy et al., 2005) and the Rsc4(36-321) fragment as a search model. Model building was

performed using COOT (Emsley and Cowtan, 2004), and refinement with TLS

parameters was performed using REFMAC as implemented in CCP4i (1994). TLS

parameters were generated using the TLSMD server (Painter and Merritt, 2006).

Microarray Analysis

RNA was prepared from strains YBC2898 and YBC2899 grown at 33°C in SD

supplemented with lysine, methionine, histidine, leucine, and uracil and labeled using the

Agilent Low RNA Input Linear Amplification kit. Labeled samples were applied to a

four-pack yeast expression slide (Agilent, catalog # G2519F AMADID 015072).

Hybridization, washes, data extraction and normalization were performed according to

manufacturer's protocol. Data from four independent experiments were averaged and the

resulting (mutant/wt) mean ratios are reported. Pearson correlation coefficients (r values)

were determined by plotting genome-wide expression data for one experimental replicate

versus another as a moving average (window = 5% of data set, step-size = 1) for all

possible pairwise comparisons. For each pairwise comparison $r \geq 0.90$.

RSC immunoprecipitation and antibodies

Flag immunoprecipitations for RSC assembly assays were performed by incubating 1 mg

of whole-cell extract (Cairns et al., 1999) with 20 µl bed volume of anti-Flag agarose

(Sigma) in Flag Buffer 300 (50 mM NaPhosphate [pH 7.5], 300 mM NaCl, 20 mM

EDTA, 10% glycerol, 1 mM β-mercaptoethanol, protease inhibitors) at 4°C for 3 h. The

immunocomplexes were washed four times with Flag Buffer 300, eluted by boiling with

4 x SDS sample buffer, prior to Western blot analysis. The anti-Sth1 antibody was

previously described (Saha et al., 2002). The anti-Flag antibody is from Sigma.

Supplemental Figure1

Structural Alignment of TAF1 and Rsc4-TBD overlapping BD1 domains
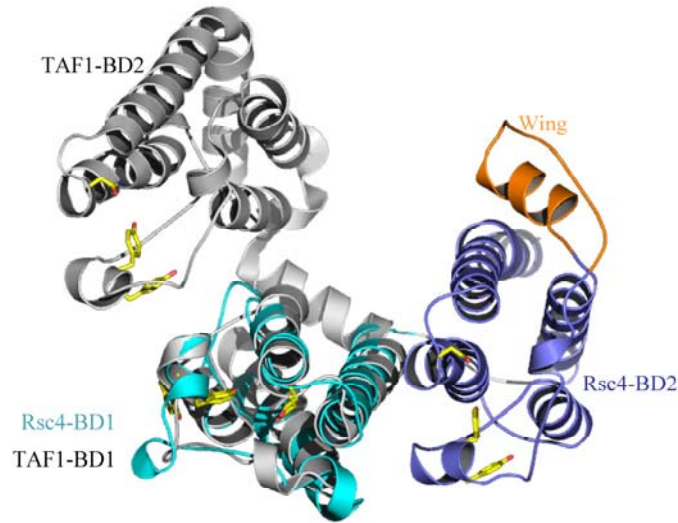
Position and orientation of TAF1 and Rsc4 bromodomains
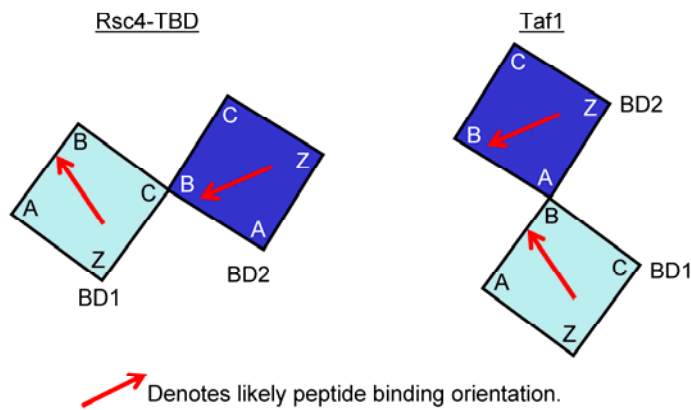
Figure S1. Structural alignment of TAF$_{II}$1 double bromodomain with the Rsc4 TBD.

Upper) Rsc4 Tandem bromodomain colored as in Figure 1B, with BD1 (cyan), BD2 (blue), Wing (orange) The TAF$_{II}$1 double bromodomain is shown in grey (Jacobson et al., 2000). Residues important for acetyl-lysine recognition indicated in yellow for both structures. Structural alignment of bromodomain 1 performed using the DALI server (Holm and Sander, 1998).

Lower) Diagram of the relative position and orientation of the Rsc4 and TAF$_{II}$1
bromodomains shown in the upper panel. Each has bromodomain 1 colored in cyan,
and bromodomain 2 in blue. The positions of the helices within each bromodomain
are indicated (A, B, C, and Z). The likely direction of a bound peptide is indicated
with a red arrow pointing from the N-terminus to the C-terminus. In the case of the
Rsc4 BD1 this arrow indicates the actual direction of the peptide containing K25ac.

Supplemental Figure 2
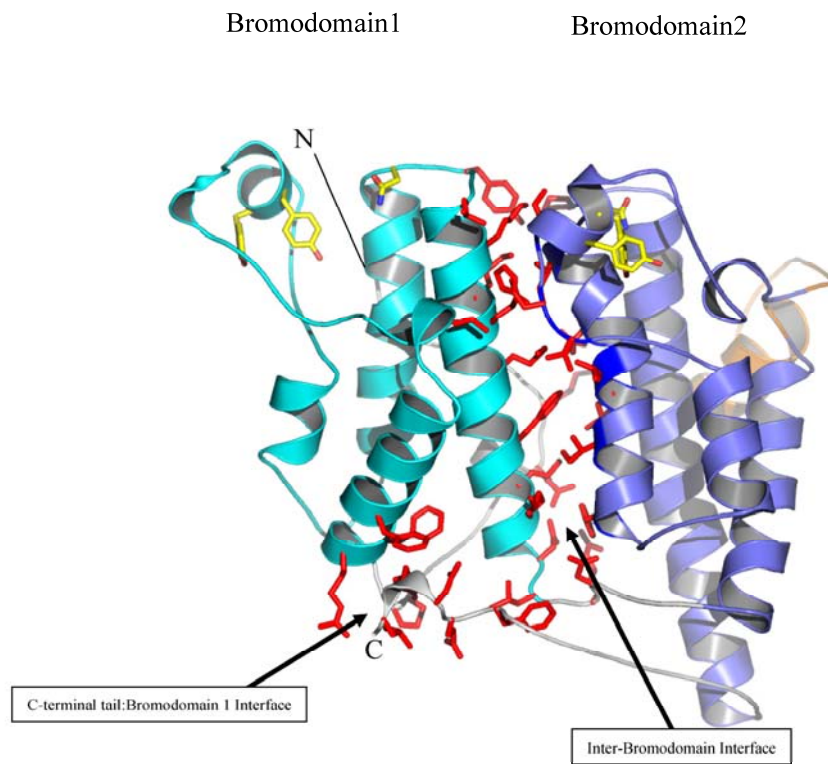
Figure S2. Tandem Bromodomain Interface.

Tandem bromodomain colored as in Figure 1B, with BD1 (cyan), BD2 (blue),
Wing (orange), and residues important for acetyl-lysine recognition indicated in
yellow. Residues that form the interface between BD1 (defined as residues 36-
162), and BD2 (residues 163-320) are shown in red.

Supplemental Figure3

Alignment by ClustalW of sequences from Bromodomains found in the PDB.

■ Highly conserved

■ Invariant

```
Rsc4BD1    DYNAPLNPKSELFLDDWHIPKFNRFISFTLDVLIDKYKD---------IFKDFIKLPSRK 87
Rsc4BD2    ----YLINSEVKAKLLHYLNKLVDATEKKINQALLGASSPKNLDDKVKLSEPFMELVDKD 220
GCN5BD     -------AMANIAQRPKR-GPHDAAIQNILT-ELQNHAA----------AWPFLQPVNKE 359
TAF1BD1    -DYLNRPHKSIHRRRTDPMVTLSSILESIIN-DMRDLPN----------TYPFHTPVNAK 1412
TAF1BD2    --LLD----------DDDQVAFSFILDNIVTQKMMAVPD----------SWPFHHPVNKK 1535
PCAF       --------GSHMSKEPRDPDQLYSTLKSILQ-QVKSHQS----------AWPFMEPVKRT 755
CBP        --------GSHMRKKIFKPEELRQALMPTLEALYRQDPE----------SLPFRQPVDPQ 1118
Brd2       ---------------GRVTNQLQYLHKVVMKALWKHQF----------AWPFRQPVDAV 106
Peregrin   --------------GSSGSSGFLILLRKTLE-QLQEKDT----------GNIFSEPVPLS 35
```

```
Rsc4BD1    FH--PQYYYKIQQPMSINEIKS-RDYEYEDGPSNFLLDVELLTKNCQAYNEYDSLIVKNS 144
Rsc4BD2    EL--PEYYEIVHSPMALSIVKQNLEIGQYSKIYDFIIDMLLVFQNAHIFNDPSALIYKDA 278
GCN5BD     EV--PDYYDFIKEPMDLSTMEIKLESNKYQKMEDFIYDARLVFNNCRMYNGENTSYYKYA 417
TAF250BD1  VV--KDYYKIITRPMDLQTLRENVRKRLYPSREEFREHLELIVKNSATYNGPKHSLTQIS 1470
TAF250BD2  FV--PDYYKVIVNPMDLETIRKNISKHKYQSRESFLDDVNLILANSVKYNGPESQYTKTA 1593
PCAF       EA--PGYYEVIRFPMDLKTMSERLKNRYYVSKKLFMADLQRVFTNCKEYNPPESEYYKCA 813
CBP        LLGIPDYFDIVKNPMDLSTIKRRLDTGQYQEPWQYVDDVWLMFNNAWLYNRKTSRVYKFC 1178
Brd2       KLGLPDYHKIIKQPMDMGTIKRRLENNYYWAASECMQDFNTMFTNCYIYNKPTDDIVLMA 166
Peregrin   EV--PDYLDHIKKPMDFFTMKQNLEAYRYLNFDDFEEDFNLIVSNCLKYNAKDTIFYRAA 93
```
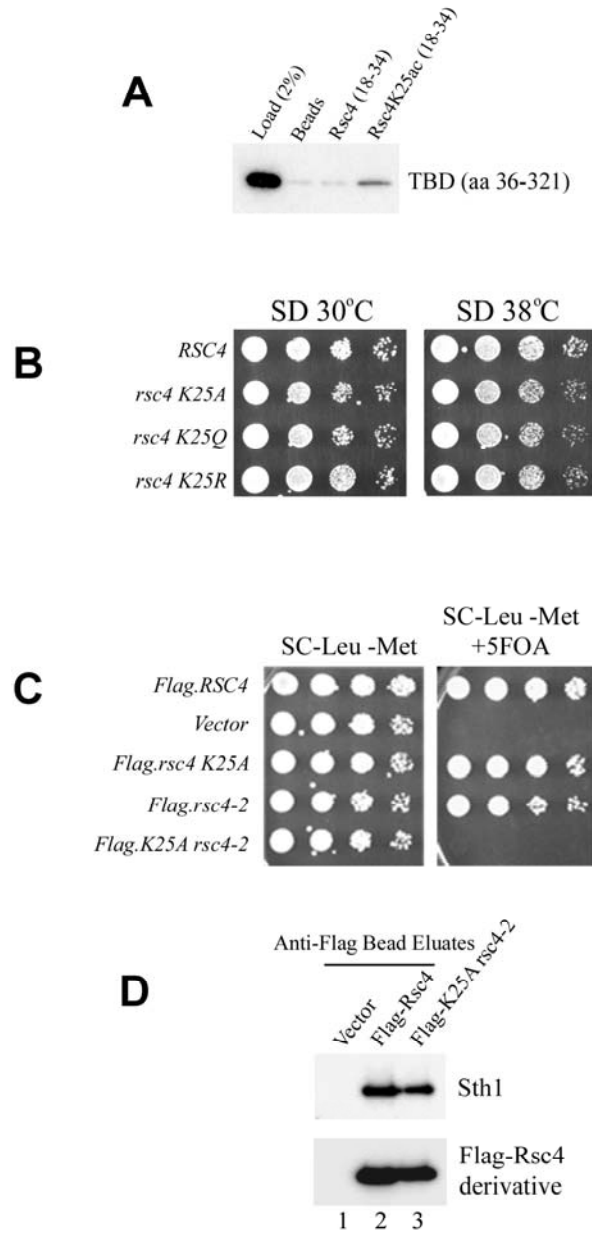
```
Rsc4BD1    MQVVMLIE----------FEVLKAKNLKRN------------ 160
Rsc4BD2    TTLTNYFNYLIQKEFFPELQDLNERGEINLEFDKFEFENYLA 320
GCN5BD     NRLEKFF----------NNKVKEIPEYSHLID--------- 439
TAF250BD1  QSMLDLC----------DEKLKEKEDKLARLEKAINP---- 1497
TAF250BD2  QEIVNVC----------YQTLTEYDEHLTQLEKDICTAKEA 1624
PCAF       NILEKFF----------FSKIKEA----GLIDK-------- 832
CBP        SKLAEVF----------EQEIDPVMQSLG----------- 1197
Brd2       QTLEKIF----------LQKVASMPQEEQELVVTIPKN--- 194
Peregrin   VRLREQG----------GAVLRQARRQAEKMGSGPSSG--- 121
```

Figure S3. Bromodomain Sequence Alignment.

Sequence alignment of a selection of structurally characterized bromodomains (aligned with CLUSTALW). Highly conserved residues (green), invariant residues (red). Residues involved in acetyl-lysine recognition (yellow dots). PDB codes for sequences are TAF$_{II}$1 (1EQF), PCAF (1JM4), CBP (1JSP), Brd2 (1X0J), Peregrin (2D9E).

Supplemental Figure 4

A

Load (2%) Beads Rsc4 (18-34) Rsc4K25ac (18-34)

TBD (aa 36-321)

B

SD 30°C   SD 38°C

RSC4

rsc4 K25A

rsc4 K25Q

rsc4 K25R

C

SC-Leu -Met   SC-Leu -Met +5FOA

Flag.RSC4

Vector

Flag.rsc4 K25A

Flag.rsc4-2

Flag.K25A rsc4-2

D

Anti-Flag Bead Eluates

Vector Flag-Rsc4 Flag-K25A rsc4-2

Sth1

Flag-Rsc4 derivative

1 2 3

Figure S4. K25 affects Rsc4 TBD function in vivo.

A) A Rsc4 peptide acetylated at K25 binds weakly to the TBD in *trans*. The format to assess binding is identical to the methods used in Figure 2. Peptides correspond to aa 18-34 of the Rsc4 sequence, either unmodified or acetylated at the Rsc4

K25, were conjugated to beads and tested for binding pure TBD (36-321). Bead washes were conducted with a buffer containing 150 mM NaCl.

B) Mutants bearing *rsc4 K25* alleles show slightly slower growth under heat stress conditions. Strains (YBC3107) bearing *TRP1*-marked *rsc4* derivatives expressed from the *MET25* promoter were spotted in ten-fold dilutions on minimal medium plates. Plates were incubated at 30°C or 38°C for 2 days. The plasmids are all *TRP1*-marked: pRS314.RSC4 (p1060); pRS314.rsc4 K25A (p2196); pRS314.rsc4 K25Q (p2198); pRS314.rsc4 K25R (p2197).

C) Growth of mutants bearing *rsc4 K25A* and a BD^{Ts-} allele. Strains (YBC627) bearing pRS316.*RSC4* or a *LEU2*-marked *rsc4* derivative expressed from the *MET25* promoter were spotted in ten-fold dilutions to selective media with and without 5-FOA to enforce loss of the pRS316.*RSC4* plasmid. Plates were incubated at 30°C for 2 days. The *LEU2* plasmids: *Flag.RSC4*, (p602); p415MET25 vector; *Flag.rsc4 K25A*, (p2360); *Flag.rsc4-2*, (p2363); *Flag.K25A rsc4-2*, (p2361).

D) Rsc4 mutant assembly into RSC. Extracts were prepared from strains as in (C) grown in the presence of pRS316.*RSC4* in SC-Leu-Ura-Met media. Immune complexes were formed with anti-Flag antibody bound resin, washed, eluted, immunoblotted, and probed with anti-Sth1 or anti-Flag antiserum.

Table S1. Genes up-regulated ≥2-fold in *rsc4K25A* mutant – only genes where 3 of 4 replicates were up-regulated ≥1.5-fold

Gene Name	Systematic Name	Mean Ratio
RTA1	YGR213C	8.461
ORF:YMR107W	YMR107W	7.746
ORF:YLL057C	YLL057C	6.480
SPS100	YHR139C	5.932
HSP30	YCR021C	5.636
ALD3	YMR169C	5.618
CMK2	YOL016C	5.207
HXT5	YHR096C	5.009
ORF:YOL014W	YOL014W	4.647
CIT2	YCR005C	4.595
HSP26	YBR072W	4.565
ORF:YML131W	YML131W	4.256
SSB1	YDL229W	4.139
ORF:YLR054C	YLR054C	3.895
DAK2	YFL053W	3.749
MET2	YNL277W	3.740
JEN1	YKL217W	3.579
SNO1	YMR095C	3.312
ORF:YBL049W	YBL049W	3.267
HBT1	YDL223C	3.256
PHM7	YOL084W	3.107
ORF:YBL048W	YBL048W	3.105
TDH1	YJL052W	3.076
TEF1	YPR080W	3.072
YPT53	YNL093W	3.062
ORF:YGR043C	YGR043C	3.050
ORF:YJL213W	YJL213W	3.049
CHS1	YNL192W	3.006
ADH6	YMR318C	2.940
PHO89	YBR296C	2.927
PUT1	YLR142W	2.821
CIT1	YNR001C	2.747
FRE1	YLR214W	2.677
NCE103	YNL036W	2.672
GYP7	YDL234C	2.668
ORF:YJL171C	YJL171C	2.661
ORF:YCR102C	YCR102C	2.654
HXT10	YFL011W	2.629
SNZ1	YMR096W	2.534
ORF:YCR007C	YCR007C	2.524
BAG7	YOR134W	2.491
ORF:YLR414C	YLR414C	2.469
PDH1	YPR002W	2.461
YDC1	YPL087W	2.459
PRM8	YGL053W	2.458
GRE1	YPL223C	2.446

ORF:YLR460C	YLR460C	2.445
KRE21	YLR338W	2.430
ORF:YER185W	YER185W	2.428
ORF:YFL061W	YFL061W	2.403
ORF:YNL335W	YNL335W	2.392
ORF:YCR100C	YCR100C	2.379
COS8	YHL048W	2.308
ORF:YHL021C	YHL021C	2.303
HXT2	YMR011W	2.290
NCA3	YJL116C	2.281
TIS11	YLR136C	2.276
ORF:YBR116C	YBR116C	2.275
PRM10	YJL108C	2.273
TKL2	YBR117C	2.257
THI4	YGR144W	2.251
ORF:YMR090W	YMR090W	2.235
BOP2	YLR267W	2.234
ORF:YDL222C	YDL222C	2.229
FET3	YMR058W	2.203
POX1	YGL205W	2.187
GCY1	YOR120W	2.175
YPK1	YKL126W	2.138
ORF:YIR044C	YIR044C	2.126
DAK1	YML070W	2.113
ASI2	YNL159C	2.108
GLR1	YPL091W	2.086
FUN34	YNR002C	2.079
SEO1	YAL067C	2.069
ORF:YGR201C	YGR201C	2.065
ORF:YAR033W	YAR033W	2.041
ORF:YOR289W	YOR289W	2.034
MSC1	YML128C	2.032
TPD3	YAL016W	2.031
TPK2	YPL203W	2.023

Table S2. Genes down-regulated ≤2-fold in *rsc4K25A* mutant – only genes where 3 of 4
replicates were down-regulated ≤1.5-fold

Gene Name	Systematic Name	Mean Ratio
SPL2	YHR136C	0.497
SRN2	YLR119W	0.496
TYE7	YOR344C	0.496
RIM4	YHL024W	0.495
HNT2	YDR305C	0.495
ICS3	YJL077C	0.493
PET100	YDR079W	0.491
ORF:YBL077W	YBL077W	0.490
SCM4	YGR049W	0.489
ORF:YDL086W	YDL086W	0.488
WSC4	YHL028W	0.486
MOG1	YJR074W	0.486
ORF:YMR122C	YMR122C	0.482
TIR1	YER011W	0.479
VPS69	YPR087W	0.479
ORF:YPR015C	YPR015C	0.477
ORF:YMR086C-A	YMR086C-A	0.474
ORF:YBR113W	YBR113W	0.471
ORF:YKR040C	YKR040C	0.469
ORF:YPL251W	YPL251W	0.467
ORF:YDR157W	YDR157W	0.466
ORF:YDR521W	YDR521W	0.461
KNH1	YDL049C	0.458
SPS19	YNL202W	0.457
SMX3	YPR182W	0.457
ORF:YKR047W	YKR047W	0.456
ORF:YBR032W	YBR032W	0.452
HMO1	YDR174W	0.451
ORF:YCR050C	YCR050C	0.450
ORF:YPL197C	YPL197C	0.449
ORF:YGR050C	YGR050C	0.446
ORF:YNL086W	YNL086W	0.438
ORF:YGL081W	YGL081W	0.436
ITR1	YDR497C	0.430
UTR2	YEL040W	0.429
PDR11	YIL013C	0.427
IST3	YIR005W	0.426
HUR1	YGL168W	0.425
ORF:YML090W	YML090W	0.425
ORF:YMR193C-A	YMR193C-A	0.412
FOX2	YKR009C	0.412
OPI3	YJR073C	0.402
CWH36	YCL007C	0.401
ORF:YDR327W	YDR327W	0.401
ORF:YMR069W	YMR069W	0.400
ORF:YLR101C	YLR101C	0.399

ORF:YKL030W	YKL030W	0.398
FAR1	YJL157C	0.382
BUD28	YLR062C	0.378
ORF:YNL040W	YNL040W	0.377
KRE20	YAL056C-A	0.372
CTR1	YPR124W	0.366
ORF:YLR198C	YLR198C	0.366
ORF:YHR049C-A	YHR049C-A	0.361
MF(ALPHA)2	YGL089C	0.361
ORF:YOR013W	YOR013W	0.359
SAG1	YJR004C	0.341
ORF:YKR049C	YKR049C	0.336
AUA1	YFL010W-A	0.331
ORF:YDL185C-A	YDL185C-A	0.256
INO1	YJL153C	0.158

Table S3. Yeast Strains

Strains	Mating Type	Genotype	Source
YBC627	*MAT* α	*rsc4Δ::HIS3 [p164;* pRS316.*RSC4] leu2Δ1 ura3-52 trp1Δ63 his3Δ200 lys2-12δ*	Kasten *et al* (2004)
LPY3430	*MAT* a	*esa1Δ::HIS3 esa1-L327S::URA3 leu2-3,112 ura3-52 trp1Δ1 his3Δ200*	Clarke *et al* (1999)
YBC1662	*MAT* α	*gcn5Δ::KanMx leu2Δ0 ura3Δ0 his3Δ1 lys2Δ0*	Research Genetics
YBC1857	*MAT* a	*sas2Δ::KanMx leu2Δ0 ura3Δ0 his3Δ1 lys2Δ0*	Research Genetics
YBC1895	*MAT* α	*leu2Δ0 ura3Δ0 his3Δ1 lys2Δ0*	Research Genetics
YBC1911	*MAT* a	*sas3Δ::KanMx leu2Δ0 ura3Δ0 his3Δ1 met15Δ0*	Research Genetics
YBC2352	*MAT* α	*gcn5Δ::KanMx rsc4Δ::HIS3 [p164;* pRS316.*RSC4] leu2Δ1 ura3-52 trp1Δ63 his3Δ200*	This work
YBC2493	*MAT* a	*hat1Δ::KanMx KanMx leu2Δ0 ura3Δ0 his3Δ1 met15Δ0*	Research Genetics
YBC2499	*MAT* a	*rsc4Δ::NatMx [p164; pRS316.RSC4] hht1-hhf1::pWZ405-F2F9-LEU2 hht2-hhf2::pWZ403-F4F10-HIS3 [p1831; H3-H4 WT; LYS2] leu2Δ1 ura3-52 trp1Δ63 his3Δ200 lys2-801 ade2-101*	This work
YBC2501	*MAT* a	Same as YBC2499 except p1832 (*h3 K14G; LYS2*) instead of p1831	This work
YBC2814	*MAT* α	*RSC2-TAP::TRP1 rsc4Δ::NatMx [p2260;* pRS412.*RSC4; ADE2] trp1::KanMx pep4::HIS3 prb1::LEU2 ade2 ura3 his3 leu2*	This work
YBC2815	*MAT* α	Same as YBC2814 except p2261 (pRS412.*rsc4 K25A; ADE2*) instead of p2260	This work
YBC1931	*MAT* a	*rsc4-2 hht1-hhf1::pWZ405-F2F9-LEU2 hht2-hhf2::pWZ403-F4F10-HIS3 [YCp-50 copy II; H3-H4 WT; URA3] ura3-52 lys2-801 ade2-101 trp1Δ63 his3Δ200 leu2Δ1*	Kasten *et al* (2004)
YBC2898	*MAT* α	*RSC4 lys2Δ0 met15Δ0 his3Δ1 leu2Δ0 ura3Δ0*	This work
YBC2899	*MAT* α	*rsc4 K25A lys2Δ0 met15Δ0 his3Δ1 leu2Δ0 ura3Δ0*	This work
YBC2822	*MAT* a	*RSC2-TAP::TRP1 gcn5Δ::KanMx pep4Δ::HIS3 prb1Δ::LEU2 leu2 ura3 his3 trp1*	This work
YBC2825	*MAT* a	*RSC2-TAP::TRP1 pep4Δ::HIS3 prb1Δ::LEU2 lys2Δ0 leu2 ura3 his3 trp1*	This work
YBC3107	*MAT* **a**	*rsc4Δ::NatMx [pRSC4; URA3] his3Δ 200 trp1Δ63 ura3*	This work

Table S4. Plasmid Constructs

Plasmid	Description
p164	pRS316.*RSC4; URA3*
pRS314	*TRP1; CEN*
p1060	pRS314.*RSC4; TRP1*
p1865	pRS314.*rsc4* (Δ187-206); *TRP1*
p1462	pRS314.*rsc4 Y92A Y93A; TRP1*
p1463	pRS314.*rsc4 Y225A Y226A; TRP1*
p1471	pRS314.*rsc4 Y92A Y93A Y225A Y226A; TRP1*
p1406	pET11a.Flag.*Rsc4TBD* (aa 46-334).10xHIS
p1567	pET11a.Flag.*rsc4TBD* (aa 46-334) *Y92F*.10xHIS
p1568	pET11a.Flag.*rsc4TBD* (aa 46-334) *Y225F*.10xHIS
p1569	pET11a.Flag.*rsc4TBD* (aa 46-334) *Y92F Y225F*.10xHIS
p1614	pET151/D.*Rsc4BD2* (aa 157-321)
p1616	pET151/D.*Rsc4TBD* (aa 1-321)
p1617	pET151/D.*Rsc4TBD* (aa 36-321)
p2296	pET151/D.*rsc4TBD* (aa 1-321) *Y92A*
p2243	pET151/D.*Rsc4TBD* (aa 1-340)
p1662	pET151/D.*Rsc4TBD* (aa 36-340)
p2515	pET151/D.*H3*(aa 6-18).Thrombin cleavage. *Rsc4TBD* (aa 1-321)
p1385	pET11a.7xHIS.*Gcn5*
p2243	p415.*MET25*.10xHIS.2xNLS.*Rsc4TBD* (aa 1-340); *LEU2*
p1831	p317.*H3-H4; LYS2*
p1832	p317.*h3 K14G-H4; LYS2*
p415.MET25	*LEU2; CEN; MET25* expression vector (methionine-repressible)
p602	p415.*MET25.Flag.RSC4; LEU2*
p2360	p415.*MET25.Flag.rsc4 K25A; LEU2*
p2361	p415.*MET25.Flag.K25A rsc4-2; LEU2*
p2363	p415.*MET25.Flag.rsc4-2; LEU2*

Supplemental References

(1994). The CCP4 suite: programs for protein crystallography. Acta Crystallogr D Biol Crystallogr *50*, 760-763.

Cairns, B. R., Schlichter, A., Erdjument-Bromage, H., Tempst, P., Kornberg, R. D., and Winston, F. (1999). Two functionally distinct forms of the RSC nucleosome-remodeling complex, containing essential AT hook, BAH, and bromodomains. Mol Cell *4*, 715-723.

Emsley, P., and Cowtan, K. (2004). Coot: model-building tools for molecular graphics. Acta Crystallogr D Biol Crystallogr *60*, 2126-2132.

Hirose, M. (1988). Effects of histone acetylation on nucleosome properties as evaluated by polyacrylamide gel electrophoresis and hydroxylapatite dissociation chromatography. J Biochem (Tokyo) *103*, 31-35.

Holm, L., and Sander, C. (1998). Touring protein fold space with Dali/FSSP. Nucleic Acids Res *26*, 316-319.

Jacobson, R. H., Ladurner, A. G., King, D. S., and Tjian, R. (2000). Structure and function of a human TAFII250 double bromodomain module. Science *288*, 1422-1425.

McCoy, A. J., Grosse-Kunstleve, R. W., Storoni, L. C., and Read, R. J. (2005). Likelihood-enhanced fast translation functions. Acta Crystallogr D Biol Crystallogr *61*, 458-464.

McRee, D. E. (1999). XtalView/Xfit--A versatile program for manipulating atomic coordinates and electron density. J Struct Biol *125*, 156-165.

Otwinowski, Z., and Minor, W. (1997). Processing of X-ray Diffraction Data Collected in Oscillation Mode. Methods in Enzymology *276*, 307-326.

Painter, J., and Merritt, E. A. (2006). Optimal description of a protein structure in terms of multiple groups undergoing TLS motion. Acta Crystallogr D Biol Crystallogr *62*, 439-450.

Saha, A., Wittmeyer, J., and Cairns, B. R. (2002). Chromatin remodeling by RSC involves ATP-dependent DNA translocation. Genes Dev *16*, 2120-2134.

Studier, F. W. (2005). Protein production by auto-induction in high density shaking cultures. Protein Expr Purif *41*, 207-234.

Terwilliger, T. C., and Berendzen, J. (1999). Automated MAD and MIR structure solution. Acta Crystallogr D Biol Crystallogr *55*, 849-861.

Van Duyne, G. D., Standaert, R. F., Karplus, P. A., Schreiber, S. L., and Clardy, J. (1993). Atomic structures of the human immunophilin FKBP-12 complexes with FK506 and rapamycin. J Mol Biol *229*, 105-124.